УДК 551.465

© *А. Ю. Бенилов*[1]*, *А. С. Сафрай*[2], *Б. Н. Филюшкин*[2], *Н. Г. Кожелупова*[2]

[1]Лаборатория прикладной физики моря, Компания «Экъют Солюшэнс», Нью Джерси, США (130 Marina Bay Court, Highlands, NJ 07732, USA)
[2]Институт океанологии им. П.П. Ширшова РАН, 117997, Нахимовский пр., д. 36, г. Москва, Россия
*e-mail: abenilov@rocketmail.com

О НЕЛИНЕЙНОЙ ДИНАМИКЕ ЛИНЗ СРЕДИЗЕМНОМОРСКОЙ ВОДЫ «МЕДДИ»

Статья поступила в редакцию 29.01.2020, после доработки 14.06.2020

Линзы средиземноморской воды, также известные как «медди», хорошо различимы в воде Атлантического океана. Полевые наблюдения, посвященные изучению «медди», представлены в многочисленных публикациях и предоставляют информацию об их происхождении, распределении, пространственных масштабах и динамической активности во времени. Солевые пальцы и двойная диффузия на верхних и нижних границах «медди» могут рассматриваться как единственные механизмы, вызывающие исчезновение «медди», как мезомасштабные термально-соленые неоднородности в окружающих водах Атлантического океана. Принимая во внимание реалистичные масштабы «медди», показано, что во временных масштабах около или менее года масса воды «медди» может считаться неизменной. Отсюда следует, что на временных масштабах менее или порядка года для «медди» справедлив закон сохранения их полной массы.

Анализ временной изменчивости «медди» проводится с использованием теоретического подхода для интрузионной линзы в стратифицированной жидкости, расширенного учётом силы Кориолиса. Центр тяжести рассматриваемых «медди» находится на уровне равной плотности. Временная изменчивость возникает из-за результирующего воздействия набора сил: избыточного давления, возникающего из-за разницы в плотности воды внутри линз средиземноморской воды и плотности окружающей среды; сил, возникающих как из-за вращения линзы (центробежная сила), так и вращения Земли (сила Кориолиса); сил, вызванных излучением внутренней волны и действием вязкости. Временная изменчивость линз средиземноморской воды состоит из двух основных этапов:

1) начальная, невязкая стадия («молодая линза»), когда баланс сил формируется силами инерции, избыточного давления, центробежной силы, силы Кориолиса и силы волнового сопротивления, вызванного излучением внутренней волны; сила Кориолиса является ключевым фактором, поддерживающим и сохраняющим компактность антициклонических линз средиземноморской воды, «медди»; она предотвращает разрушение линз средиземноморской воды, ограничивает их геометрические размеры, влияет на изменение угловой скорости линзы. Циклонические линзы средиземноморской воды дестабилизируются силой Кориолиса, их толщина уменьшается со временем, и при определенных условиях линзы средиземноморской воды могут исчезнуть как аномалии плотности уже на этой стадии;

2) стадия вязкости («старая линза») характеризуется медленным уменьшением толщины линз средиземноморской воды до ее предельного значения, которое определяется начальной толщиной и начальной стратификацией линз средиземноморской воды, а также стратификацией окружающей среды; в течение последнего периода вязкой стадии обмен теплом и соленостью с окружающей водной массой может, на характерных временных масштабах около года, существенно влиять на вырождение линз средиземноморской воды как аномалии плотности; на этой стадии антициклонические линзы средиземноморской воды, «медди», продолжают иметь антициклоническое вращение.

Ключевые слова: линзы средиземноморской воды, «медди», временная изменчивость, теоретический подход, невязкая стадия, сила Кориолиса, вязкая стадия, стратификация

© *A. Yu. Benilov*[1]*, *A. S. Safray*[2], *B. N. Filyushkin*[2], *N. G. Kojelupova*[2]

[1]Applied Marine Physics Lab, Acute Solutions, 130 Marina Bay Court, Highlands, NJ 07732, USA
[2]Shirshov Institute of Oceanology RAS, 117997, Nahimovsky Prospekt, 36, Moscow, Russia
*e-mail: abenilov@rocketmail.com

ON NONLINEAR DYNAMICS OF MEDDIES

Received 29.01.2020, in final form 14.06.2020

The lenses of the Mediterranean water (LMW), also known as Meddies, well distinguishable in the Atlantic Ocean water. The field observations devoted to study Meddies are presented in numerous publications and provide information on their origination,

Ссылка для цитирования: *Бенилов А.Ю.*, *Сафрай А.С.*, *Филюшкин Б.Н.*, *Кожелупова Н.Г.* О нелинейной динамике линз средиземноморской воды «медди» // Фундаментальная и прикладная гидрофизика. 2020. Т. 13, № 3. С. 20–42. doi: 10.7868/S2073667320030028

For citation: *Benilov A.Yu.*, *Safray A.S*, *Filyushkin B.N.*, *Kojelupova N.G.* On Nonlinear Dynamics of Meddies. *Fundamentalnaya i Prikladnaya Gidrofizika*. 2020, 13, 3, 20–42. doi: 10.7868/S2073667320030028

distribution, spatial scales and temporal dynamic activities. The salt-fingers and double-diffusion at the Meddies top and bottom borders may be considered as only mechanisms causing the Meddies disappearance as the thermal — saline mesoscale anomalies in the surrounding Atlantic Ocean waters. Taking into account the Medies' realistic scales it is shown that in temporal scales of about and less than a year the Meddies water mass may be considered as invariable. Then the Meddies conservation mass is valid in such temporal scales.

The Meddies (LMW) temporal variability analysis is carried out using the theoretical approach of intrusive lens in stratified fluid extended taking into account the Coriolis force. The Meddies (LMW) are considered with the center of gravity sitting at the level of equal density. The temporal variability occurs due to the resulting effect of the set of forces: the surplus pressure originated due to the density difference between the water inside the LMW and the ambient density field; the forces originated due to both the lens' rotation (centrifugal) and the Earth rotation (Coriolis); the forces caused by the internal wave radiation and the viscosity action. The temporal variability of LMW constitutes of two principal stages:

1) the initial, inviscid stage ("young lens"), when balance of forces is formed by the forces of inertia, the surplus pressure, the centrifugal force, the Coriolis force and the force of wave resistance due to the internal wave radiation; the Coriolis force is a key factor supporting and keeping compact the anti-cyclonic LMW, the Meddies; it prevents the LMWs from breakup, limits their geometrical dimensions, affects the lens angular velocity variations. The cyclonic LMWs are destabilized by the Coriolis force, getting small thickness and under certain conditions may disappear as a density anomaly already at this stage;

2) the viscid stage ("old lens") is characterized by a slow decreasing of the LMW thickness up to its limit value, that is determined by the LMW initial thickness, the initial LMW stratification as well as ambient stratification; during the final period of the viscous stage the exchange of heat and salinity with ambient water-mass may, on a characteristic temporal scales about a year, significantly influence on the degenerations of the LMW as a density anomaly; at this stage the anti-cyclonic LMW, the Meddy, continues to have the anti-cyclonic rotation.

Key words: lenses of the Mediterranean water, Meddies, temporal variability, theoretical approach, inviscid stage, Coriolis force, visid stage, stratification

1. Meddies Origination, Distribution and Spatial-Temporal Scales

One of the most interesting and prominent features of the North Atlantic Ocean is the salt tongues originating from an exchange flow between the Mediterranean Sea and the Atlantic through the Strait of Gibraltar. The Mediterranean outflow through the strait is denser than Atlantic water because of its higher salt content. Evaporation in the Mediterranean Sea raises the salinity to around 38.4 PSU, as compared with 36.4 PSU in the eastern North Atlantic [1]. The flux of the warm and saline Mediterranean Water (MW) into the North Atlantic Ocean through the Strait of Gibraltar is about in magnitude on the order of 1 $Sv = 10^6\ m^3\ s^{-1}$[2–4], and also is one of several distinct water sources whose interactions determine the overall watermass distribution of the North Atlantic.

Mediterranean Water (MW) flows through the Strait of Gibraltar as an undercurrent, cascades down the continental shelf, while entraining less dense North Atlantic Central Water [5] and settles at depths between 500 and 1500 m [6]. MW are distinguished by high temperature and salinity, which are changed accordingly from 38 PSU and 14 °C in the Gibraltar strait up to 36.8 PSU and 13 °C in the area of the Gulf of Cadiz. Also, the influx of the Mediterranean Water as a jet (36.5 PSU salinity, 12 °C) was revealed using data of 3 surveys in the translating westward and rotating anti-cyclonically. This phenomenon led to formation of asymmetric dipole lenses system: anticyclones (western) and cyclones ones [7, 8]. Meddies were first reported in the western North Atlantic Ocean where the Mediterranean Water in the form of an intense Mesoscale Eddy had been detected off the Bahamas by McDowell and Rossby [9] and later in Sargasso Sea by Dugan, Mied, Mignerey and Schuetz [10]. Since that time Meddies have been found as a common feature in the North Atlantic Ocean [11–15], [6], [16], [17]. The distribution of Meddies detected in historical data of the eastern North Atlantic relate to the area (25°—45°N, 5°—32°W). Transformation of the Mediterranean Water jet momentum into the vortex dipole gave rise to a so called "mushroomlike" structure [18–21]. Mushroomlike structures of such a kind were also repeatedly observed in laboratory experiments [18, 20, 22, 23, 24]. Many different aspects of Meddies are currently being researched to understand their properties as well as their influence on large-scale mixing and climate [25, 26].

The hydrological and dynamical properties of several Meddies south of 40°N have been thoroughly described [12, 27–32]. The Meddies are roughly circular lenses with thermohaline anomalies of typical diameter 30–100 km and thickness 500–1000 m, centered near a depth of 1500 m. Away from the Iberian Peninsula, maximum anomalies of temperature and salinity relative to their environment can reach 5 °C and 1 PSU. Meddies have a steep boundary in hydrological properties located at a radius of 10–40 km, thus defining the ''core'' and the ''outside'' of the lens. Within the core, the velocity distribution is close to a solid body rotation, and maximum azimuthal velocities are reached at radii slightly smaller than that of the steepest hydrological front. The outside region is characterized by a sharp decrease of azimuthal velocities and by thermohaline intrusions and hydrological inversions resulting from mixing, whereas the core is smooth and stably stratified. Vertical displacements of isopycnals tend to be larger below

the core than above, and there is evidence that Meddies can have a signature extending up to the sea surface [33, 28, 32]. Meddies occasionally exhibit a ''double core'' vertical structure, with two maxima in temperature and salinity anomalies.

Meddies have traditionally been studied using established oceanographic techniques, such as CTD (Conductivity-Temperature-Depth) probes to measure salinity and temperature [34] and acoustically tracked SOFAR floats [27]. A multi-channel seismic (MCS) reflection profiling has been employed as an imaging tool [35–40]. Biescas et al. [37] performed the first detailed MCS analysis of a Meddy. Buffett et al. [40] combine the MCS analysis with the Stochastic Heterogeneity Mapping to the study of a Meddy in the Gulf of Cadiz.

In its crossing of shelf canyons the sink of denser MW along the canyon bottom on the 800–1400 m occurs. The isolated volumes of MW are well distinguishable from surrounding water in salinity (up to 0.6 PSU) and temperature (up to 3 °C). This leads to formation of dipole systems of different scales with two intrathermocline eddies — cyclonic and anticyclonic. The data obtained in the course of the cruise of R/V "Vityas" in 1988 [41; 7; 21] show successive increasing of MW inflow as a jet (36.5 PSU salinity, 12 °C) that was revealed using data of 3 surveys in the open part of the ocean, remote from the Iberian Peninsula continental slope more than 250 km at intermediate 700–1300 m depths. This phenomenon led to formation a vortex dipole of the MW lenses system: anticyclones (western) and cyclones ones [7]. The Coriolis force acts as a stabilizing factor for lenses with anticyclones rotation, prevents their decay and restricts its geometry dimensions and circulation velocity. The lenses rotate with a frequency commensurable with Coriolis parameter [42]. These lens' characteristics are determined by the balance of the surplus of centrifugal force and Coriolis force and depend on the initial potential energy of the lenses and its angular momentum. Lenses with the cyclone circulation are destabilized by Coriolis force, they quickly spread in a horizontal plane and their vertical sizes decrease. The collapse of cyclonic lenses occurs in vicinity of the region of their formation and their lifetime is approximately estimated as long as 60 days [43]. This process is the main mechanism of lenses material exchange with the surrounding waters and formation the intermediate MW in the close vicinity of their inflow into the Atlantic Ocean.

The laboratory experiments well qualitatively support the observed "young" eddies in the Gulf of Cadiz. The transformation of the MW jet momentum into the sequence of the vortex dipoles which manifest themselves as the sequence of the "mushroomlike" coherent structures [19]. The mushroomlike structures of such a kind were also repeatedly observed in laboratory experiments [18, 20, 22, 23]. The propagation of these waters into the North Atlantic plays an important role in the ocean thermo-mass- energy exchange. The most of characteristics of this layer have noticeable horizontal irregularity. For instance, the sizes of the high salinity regions within the Mediterranean water layer may have scales of tens kilometers. This kind of lenses are observed at distances up to 3×10^3 km from the source of the Mediterranean water in the Atlantic Ocean and move with a speed of about ~1.0–1.4 nautical mile/day. This observed evidence shows that the lenses of the Mediterranean water are the long — living formations with a lifetime at least several years. The lifetime of the lens observed during the Mezopoligon experiment [42] has reached about 6 years. The large-scale current system at those depths transports the lenses of the Mediterranean water across the ocean [44, 45]. The observations in the ocean region near the Iberian Peninsula have shown that an appearance of about 50 lenses per year is possible [41, 46]. Then we obtain that the region with a horizontal scale of ~1800 km from the Gulf of Cadiz is populated by the lenses drifting with velocity of 1.0 mile/day during of 3 years and so about 150 lenses may be observed at every moment. The density structure of the lens water-body is characterized by higher vertical mixing relatively to that within surrounding fluid [27, 47]. The difference between the lens density distribution and the surrounding water masses produces a horizontal gradient of pressure surplus that is the intrusion driving force causing the lens spreading at the depth where the lens mean density is equal to the ambient density.

The presence of salinity and temperature maximums within lens creates favorable conditions for developing two kinds of convective phenomena at the upper and bottom boundaries: the double-diffusion at the top boundary and the "salt-finger" at the bottom and turbulent exchange at outer boundaries with thermohaline lateral intrusions. Estimates of the vertical heat and salt transfer produced by those phenomena show the values of effective coefficients for both heat K_{zT} and salt K_{zS} less than 1 cm^2/s [27]. It should be noted that those estimates relate to the "young" lenses located near their originating source. Because of the convective phenomena at the lens boundaries there is an exchange between the lens seawater and the ambient seawater by the heat and the salt that induces degeneration of the lens as temperature and salinity anomalies. The double-diffusive and salt-finger convection captures the surrounding fluid, which has ambient values of temperature and salinity. The lens anomalies of temperature and salinity diminish in time as the result of this exchange with ambient water [43].

This process of heat and salt exchanges was irregular in time during the monitoring the lens "Sharon" [27]: during the first year (about 300 days) the lenses lost 2/3 of its heat and salt, and in remaining two years it lost only 1/3 of them. It should be noted that the lenses "Sharon" was revealed in the Azores front region, and its age could

be estimated in 2–3 years. How did its destruction occur, and what were heat and salt losses before this period was unknown. Furthermore there are more rapid mechanisms of heat and salt transfer from lenses to surrounding waters: 1) partial destruction (damages) of lenses in their meeting (as a result of collisions) with underwater mountains [48], 2) their (passage) moving in straits (through underwater canyons) [49], 3) their interaction with frontal zones [50], 4) lenses destruction on periphery of strong streams [51].

Two stage of anticyclonic lens evolution are revealed: 1) as a rule the "young" lenses form a vortex dipole system and may have two cores structure along vertical because the lens formation is not finished (fig. 1); 2) the "old" lens has one formed core, and there is no trace of cyclonic lens. The anticyclonic lenses are called "Meddy" (Mediterranean Eddy) in literature; they carry main MW volumes at periphery of the area and determine the scales of thermohaline inhomogeneities. These lenses are closed ellipsoidal formations with horizontal axes of 40–100 km and vertical ones of 0.4–0.9 km; MW volumes in them are up to 3500 km^3.The average MW volume is 1720 km^3 for 178 lenses [43].

The observations facts in a summarized form can be presented as follows:

a) MW enters in the Atlantic Ocean through the Gibraltar strait by a bottom current, occupies depth about 800–1500 m and forms a layer of intermediate MW. The layer extends across the ocean up to 3000 km and at the same time it is the two-component system: water with typical MW characteristics are saturated by greater number of lenses, fulfilled by MW water with higher values of TS-indexes and noticeably distinguished from surrounding waters.

b) Main heat and salinity transport by MW at intermediate depths at long distance from the source of their origin is determined by the processes of formation, spread and decay of intrathermocline anticyclonic lenses. We may call them as "old lenses" or Meddy. The cyclonic lenses do not travel far because they collapse under destabilizing acting the horizontal surplus pressure gradient and the centrifugal and Carioles forces. Their life time from the observation is estimated approximately no more 60 days. This process is the main mechanism of lenses water mass exchange with the ambient waters and formation MW layer in the close vicinity of the region of the MW lenses origination.

c) The "young" lenses of the Mediterranean water are the lenses which occur as cyclonic — anticyclonic pairs at relatively near to the Mediterranean water-forming source, the anticyclonic lens is well expressed while the cyclonic lens is less expressed and has greater horizontal scale. The mechanism of the "mushroomlike" dipole system generated along with inflow of MW is an unstable stream at intermediate depths. It seems to be common one in the open ocean as well as in the "sinking" water in canyons.

The models of lens dynamics have been elaborated [see for example 10, 21, 25, 52–57, 60]. The interaction of Meddies with a complex distribution of seamounts is studied in the three-layer quasi-geostrophic model on the *f*-plane [58]. This study aims at understanding if and how this seamount chain can represent a barrier to the propagation of these eddies and how it can be involved in their decay.

In this paper we focus mostly on the lens dynamics during the lens lifetime following the results in [21, 41]. First, we estimate the characteristic temporal scale of the lens degradation as a thermohaline departure from the ambient water. Second, we analyze the lens dynamics itself.

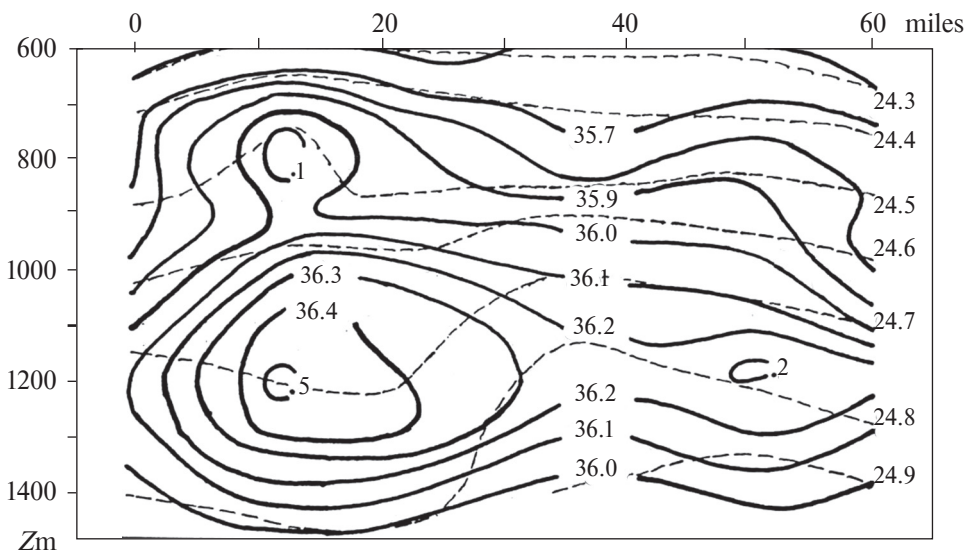

Fig. 1. Distribution of salinity (PSU) on the vertical section drawn through the centers of dipole lenses (solid lines). Density (σ_t) is shown by dashed lines. Corresponding data were obtained during the period June, 22–26, 1988 by R/V "Vityaz" [7, 41].

2. The Lenses Decay

Our goal is to find the order of magnitude of the time-scale of the lens degradation. The mass exchange between the lens and the ambient water defines the rate of lens decay as a temperature — salinity departure. We make a rough estimate of the characteristic rate of the seizing the ambient water mass around the lens using the estimates of the effective coefficients K_{zT} and K_{zS} in [27]. According to the observation we may assume that the lens thickness $2h$ (h is the lens semi-thickness) is much less than the lens horizontal scale $2R$ (R is the lens radius) and the ratio $R^{-1}h$ has the order of magnitude as $R^{-1}h \le 10^{-1}$. In this case the estimates can be done for an infinite in horizontal directions layer, which extends in vertical direction by the water mass exchange with the ambient water. Because we are not interested in detail of the lens decay but looking for estimates by the order of magnitude, this approach allows us a simplification of the problem introducing few additional assumptions:

1. The ambient temperature (T_{am}) and salinity (S_{am}) are constants.
2. The lens temperature (T_λ) and salinity (S_λ) depend only on the time t.
3. The effective diffusivity coefficients K_{zT} and K_{zS} have the same order of magnitude at the upper lens border and the lens bottom and can be taken as

$$K_{zT}(h) \approx K_{zT}(-h) \approx K_{zS}(h) \approx K_{zS}(-h) \approx K_z = \max\left(K_{zT}, K_{zS}\right). \tag{1}$$

These assumptions will provide most intensive mass exchange between the lens and the ambient water. In fact, the condition (3) means that the heat and salt transfer within upper and lower part of lens is symmetrical. Then we can take for analysis only a half of lens thickness, let say it will be the upper half, putting the origin of coordinates at the middle of lens layer and taking a vertical direction as positive for the vertical coordinate z. The change of the lens temperature, (T_λ), and salinity, (S_λ), in time is given by the equation

$$d_t\theta_\lambda = -\partial_z Q_\theta,\ |z| \le h, t \ge 0,\ \theta_\lambda = (T_\lambda, S_\lambda),\ Q_\theta = Q_\theta(z,t), \tag{2}$$

where $Q_{\theta=T}$ is the temperature (heat) flux, $Q_{\theta=s}$ is the salinity flux. The left hand side in (2) does not depend on the vertical coordinate z, and there is symmetry of the heat and salt exchange at upper and bottom sides of the lens, therefore the flux Q_θ has the form

$$Q_\theta(z,t) = zh^{-1}Q_\theta(h,t), \tag{3}$$

where Q_θ is the flux at $z = h$. Keeping fluxes of heat and salt to be continuous across the lens border we have to equalize fluxes by the entrainment with the entrainment speed $d_t h$ and by the effective diffusivity. Then the fluxes $Q_\theta(h, t)$ can be presented by the equations

$$Q_\theta(h,t) = -\left[\theta_a - \theta_\lambda(t)\right] d_t h \approx -K_z\left[\theta_a - \theta_\lambda(t)\right]/h. \tag{4}$$

The outcomes of (3) are an expression for the lens thickness h and, accordingly, an expression for the entrainment speed $d_t h$ as

$$h(t) = h_0\sqrt{1 + 2K_z t h_0^{-2}}, \tag{5}$$

$$d_t h = K_z\left(h_0\sqrt{1 + 2K_z t h_0^{-2}}\right)^{-1}, \tag{6}$$

where h_0 is the lens thickness at the time $t = 0$. Equations (5)—(6) allow an estimate of $d_t h$ taking into account the estimate of K_z of [27] and an actual value h_0. Assuming $K_z \approx 1$ cm^{2}s^{-1} and $h_0 \approx 3 \times 10^4$ cm, we find $d_t h \le 3 \times 10^{-5}$ cms^{-1}.

Let us now estimate the degradation time, t_d, of the lens anomaly which we shall take, for certainty, as the time of ten times decrease of the magnitude of lens thermohaline anomaly. Substitution the flux Q_θ of (3) in the equation (2) with taking into account (4)—(6) reduces (2) to an equation in respect to θ_λ as follows

$$d_t\theta_\lambda = -K_z\left[\theta_\lambda(t) - \theta_a\right]\left[h_0^2\left(1 + 2K_z t h_0^{-2}\right)\right]^{-1}. \tag{7}$$

The solution of (7) in the form of decay of the lens anomaly $\delta\theta = \theta_\lambda - \theta_a$ is

$$\delta\theta / \delta\theta_0 = \left(1 + 2K_z t h_0^{-2}\right)^{-1/2}, \tag{8}$$

where $\delta\theta_0 = \delta\theta(0)$ is the initial magnitude of the lens anomaly $\delta\theta$. Introducing the notation $\delta\theta_{t_d} = \delta\theta(t_d)$ and resolving (9) in respect to t_d we find the lens degradation time

$$t_d = h_0^2\left[\left(\delta\theta_0 / \delta\theta_{t_d}\right)^2 - 1\right] / 2K_z \tag{9}$$

as a function of the degradation measure $\delta\theta_{t_d} = \delta\theta_0$. If we put $\left(\delta\theta_{t_d} / \delta\theta_0\right) = 0.1$ then the degradation time t_d is about $t_d \approx 1.427 \times 10^3$ years. Hence, the lens motions with temporal scales much less than t_d and with velocities much higher than $d_t h$ of (6), as it follows from the above estimates, will not be affected by the double-diffusion and the salt-finger convection, those can be neglected if we consider more realistic time-scales and actual velocities of the lens water mass change. For instance, the lens changes for a year under this kind of erosion are $(h/h_0) \approx 1.03$, $\left[\left(d_t h\right) / \left(d_t h\right)_{t=0}\right] \approx 0.97$, $(\delta\theta/\delta\theta_0) \approx 0.97$.

Let us now estimate the lens degradation assuming, that the lens evolution occurs as a result of the lens water mass interaction with a small- scale, in respect to the lens scales, random and spatially-statistically uniform ambient dynamic noise. In this situation the effect of the small-scale components of motion on the large-scale motion will become apparent as a diffusive spreading of the large-scale non-uniformities by the small-scale motions [59]. Also, we shall make a distinction between vertical and horizontal exchange, resulting as the stable stratification effect, introducing a difference of the vertical and horizontal diffusivities. Then, the simplest model to estimate this degradation mechanism of the lens temperature and salinity anomalies takes the form of the 3-D diffusion model

$$\partial_t \delta\theta = K_z \partial^2_{zz} \delta\theta + K_L \Delta\delta\theta, \tag{10}$$

where K_z is the vertical diffusivity, K_L is the horizontal diffusivity, Δ is the horizontal Laplacien. The maximum of the lens anomaly is at the lens center $z = x = y = 0$ and decays in time as

$$\theta(t,0,0,0) / \delta\theta_0 \approx \left(h_0 / \sqrt{\pi t K_z}\right) \times \left(S_0 / 4\pi t K_L\right), \tag{11}$$

where $h_0 = h(0)$ is the initial semi-thickness of the lens, S_0 is the lens initial area in the horizontal (x, y)-plane.

The right-hand side of (11) is a product of two factors. The first term is the anomaly degeneration by the vertical mass exchange. It is similar to that of the formula (8) for $K_z t h_0^{-2} >> 0.5$. One can consider that K_z is induced by small-scale turbulence that causes the vertical transport with the coefficient $K_z \approx 1$ cm^2/s under the condition of stable stratification. Then the role of vertical diffusion in the degeneration of the anomaly $\delta\theta$ is the same as the double-diffusion and salt-fingers make. This effect is insignificant for temporal scales about one year for the actual lens with $h_0 \approx 3 \times 10^4$ cm.

The second factor describes the anomaly degradation by the horizontal diffusion. For actual area S_0 that is $S_0 \approx 3 \times 10^3$ km^2, time scales about one year an appreciable influence of the horizontal diffusion will be caused by the coefficient K_L if it is $K_L \approx 10^6$ cm^{2}s^{-1} or greater. This value of the coefficient K_L is a commonly excepted number in the large-scale oceanic currents modeling. However, it is well known that this value of the coefficient K_L is caused by the horizontal turbulent motions with scales of the same order of magnitude of that the actual lenses have, and, therefore, cannot affect the lens degradation. Thus, the introducing into consideration the horizontal diffusion does not appreciably contribute into the lens degradation process at the temporal scales of 1 year or less.

The above discussion demonstrates that the mass-exchange between the lens and the ambient water mass does not change much the total water mass confined within the lens body. As one can see in the equations (8), (10), the lens degradation rate by the mass-exchange can significantly increase if the lens thickness becomes small enough. Inside the lens body the density of seawater is more uniform over the lens volume than the density of the ambient oceanic water. Also, the lens rotates around its vertical axis and spreads in the horizontal (x, y) — plane, therefore the lens has to collapse at the depth of its density under impact of the pressure excess and the centrifugal force. However, the lens is not fully mixed and, therefore, will experience incomplete collapse. As it follows from the laboratory experiments [15] and theoretical study [4] of the collapse of such stratified regions, the lens collapses up to a final thickness $h = h_{cr} = h_0\left[\Gamma_{\rho\lambda}(0) / \Gamma_{\rho am}\right]$ (where h_0 is the initial thickness of the collapsing region, $\Gamma_{\rho am}$ is the ambient vertical gradient of density, $\Gamma_{\rho\lambda}(0)$ is the initial vertical gradient of density of the mixed region or inside the lens) and the lens' density gradient $\Gamma_{\rho\lambda}(t)$ becomes equal to the ambient density gradient $\Gamma_{\rho\lambda}/\Gamma_{\rho am}$, and the lens as a density anomaly disappears. According to the data [9], the ratio $\Gamma_{\rho\lambda}/\Gamma_{\rho am}$ can have the numerical value as up to $\Gamma_{\rho\lambda}(0)/\Gamma_{\rho am} \approx 0.1$, and then h_{cr} is ten times less than h_0. Replacing h_0 by h_{cr} in the equations (8) and (11), taking into account that $h_0 = h_{cr}\left[\Gamma_{\rho am} / \Gamma_{\rho\lambda}(0)\right]$, and assuming that h_0, K_z and $\overline{K}_z$ take the same numerical values as before, we find $\delta\theta/\delta\theta_0 \approx$ ≈ 0.35 by the double-diffusion and salt-finger convection and $\delta\theta/\delta\theta_0 \approx 0.1$ by the erosion caused by the small-scale turbulence. Thus, the collapse effect is an important part of the lens dynamics modeling.

3. The Lens Dynamics

Below the lens dynamic model is an extension of the collapse mechanism of mixed regions in a stratified fluid [54–56] with rotation. The rough preliminary estimates show that the lens collapsing process is an important element in the time-history of the Mediterranean lenses. In addition, the existing models are too complicated to carry out a qualitative analysis on revealing dynamic causes of the Mediterranean water localization within a confined region. Therefore, it would be expedient to develop a simplified model of the intrusive lens that makes possible to carry out this analysis in most clear form and, at the same time, to take into account all specific features of this phenomenon. We will discuss a variant of such coarse model, based on the theory of collapsing mixed regions in a stratified fluid [21, 54–56, 61, 62]. Also, this theory describes the lens evolution while the lens rotation is totally decayed.

Keeping in mind the results of Section 2, we assume the exchange of lens heat, salt and all other admixtures with the ambient water is so insignificant that it can be neglected at the temporal scales of the lens dynamic variability, which are the subject of interest here. Then, the lens volume characterized by total surplus of heat and salt against to those in the surrounding water mass does not change in time, or the lens volume is

$$V = 2h(t)\pi R(t)^2 = \text{const}, \tag{12}$$

where V is the lens volume, h is the lens semi-thickness, and R is the lens radius. In the case when the lens does not rotate and the Coriolis parameter $f = 0$, the lens time history obeys to the equation of a collapsing density non-uniformity in stratified fluid [55, 56]. In the terms of our problem this equation is

$$\rho_H \frac{d^2R}{dt^2} = F_g + F_w + F_{vr} \tag{13}$$

where ρ_H is the seawater density at the depth H for both within the lens and the ambient water mass, and the right hand side is a sum of three forces. The first one, F_g, is the force by the pressure surplus due to differences of the vertical density distributions in the lens water mass and the ambient water. The second force, F_w, is the force of wave-resistance due to internal wave generation during the lens intrusion process. The third force, F_{vr}, is the viscous resistance due to the lens intrusion into the calm ambient water. Because the lens axial symmetry and the horizontally uniformity of the ambient water, the forces are only along the lens radius. The force of the pressure surplus is outward as the intrusion moving force, while the resistance forces are inward to the lens center and against the intrusion motion. We specify the forces F_g, F_w and F_{vr} following [55, 56] as

$$F_g = -\frac{\Delta P}{R},\ \Delta P = -\frac{1}{3}\rho_H\left[h(t)N_{am}\right]^2\left[1-\sigma\frac{h(0)}{h(t)}\right],\ \sigma = \frac{N_{\lambda 0}^2}{N_{am}^2}, \tag{14}$$

$$F_w = -k_w\rho_H\left(h/R\right)N_{am}\left(dR/dt\right), \tag{15}$$

$$F_{vr} = -k_v\rho_H h(t)^{-2}\left(dR/dt\right)^2, \tag{16}$$

where ΔP is the pressure surplus, $R(t)$ is the lens radius, $h(t)$ is the lens semi-thickness at the time moment t and the $2h(0)$ is the lens initial thickness, σ is the lens mixing parameter equaled to zero for the fully mixed lens and it is in the range $0 \le \sigma < 1$ depending on the Brunt — Väisälä frequencies of the ambient water mass N_{am} and the lens $N_{\lambda 0}$ at the initial time $t = 0$, k_w and k_v are the dimensionless coefficients of the wave and viscous resistances correspondingly and, quantitatively, they have the order of magnitudes of 1. The different stages of lens collapse, following from (12)—(16) in this simplest case, are investigated in [55, 56] and they are well supported by the laboratory experiments (see references in [55, 56]). Here we note an important feature of lens collapse that will be used in farther discussion. In the case of incomplete mixing of the lens water mass, $0 < \sigma < 1$, the lens spreads in horizontal plane until the lens thickness reaches its critical value $h = h_{cr} = \sigma h_0$, and that corresponds to the lens' finite horizontal size $R = R_{cr} = R_0/\sigma^{1/2}$ because of the lens volume conservation (12). In the case fully mixed lens, $\sigma = 0$, the lens collapses completely, the lens thickness $2h \to 0$, but this process is very slow as the horizontal size $R(t)$ increases in time as $R(t) \sim t^{1/10}$.

We complicate the problem adding to the collapse process (13)—(16) the lens rotation with an angular velocity ω parallel to the vertical coordinate z. In this case the lens dynamics equation (13), that takes into account the forces in the radial direction, should be supplied with an equation for the lens angular velocity ω. Then we have to take into account two components of the Coriolis force of the lens own-rotation, the radial and azimuthal components. They occur due to the intrusion the lens water mass into the ambient water in the radial direction and the lens own-rotation. Also, the lens own-rotation causes the azimuthal component of the viscous resistance. It is convenient for making farther analysis in terms of the radial velocity $v_r = dR/dt$ and the azimuthal velocity $v_\varphi = R\omega$, $\omega = |\boldsymbol{\omega}|$. Using this notation the rotating lens dynamics extends to the set of two equations:

$$\rho_H \frac{d^2R}{dt^2} = F_g + F_w + F_{Cr} + F_{vr}, \tag{17}$$

$$\rho_H \frac{dv_\varphi}{dt} = \rho_H \frac{dR\omega}{dt} = F_{C\varphi} + F_{v\varphi}, \tag{18}$$

where the forces F_g, F_w and F_{vr} are defined by the equations (14)—(16), and the forces F_{Cr}, $F_{C\varphi}$ and $F_{v\varphi}$ are equal correspondingly to

$$F_{Cr} = \rho_H R\omega^2, \tag{19}$$

$$F_{C\varphi} = -\rho_H \omega\left(dR/dt\right), \tag{20}$$

$$F_{v\varphi} = -k_v \rho_H v \frac{R\omega}{h^2}. \tag{21}$$

One can see that the radial component of the Coriolis force is the centrifugal force accelerating the lens intrusion and collapse. The azimuthal component of the viscous friction reduces the lens rotation. The azimuthal component of the Coriolis force occurs due to the radial intrusive spreading of the lens water mass.

In the course of the initial inviscid stage the viscous friction can be neglected in (17) and (18). Then the equation (18) reduces to

$$\frac{dR\omega}{dt} + \omega\frac{dR}{dt} = 0, R^2\omega = L = \text{constant}, \omega = 2\pi\left(L/V\right)h \tag{22}$$

and this is the conservation of the lens angular momentum L in the absence of viscous forces. The angular velocity ω is the decreasing function of the lens radius during the inviscid stage. In the case of completely mixed lens, $\sigma = 0$, the angular velocity ω decreases to the zero value ($\omega \to 0$) because $h \to 0$ and $R \to \infty$. In the case of incomplete mixed lens, $0 < \sigma < 1$, the lens thickness decreases up to the lens limit thickness $h = h_{cr} = \sigma h_0$. This limit situation can be reached, under certain conditions, in the course of the inviscid stage and then density anomaly disappears but the liquid inside the lens continues to rotate with the limit angular velocity $\omega = \omega_{cr}$, $\left(\omega_{cr} = LR_{cr}^{-2} = \sigma LR_0^{-2}\right)$. The temperature and salinity anomalies, which compensate contribution of each other in the stably density stratified lens, are lasting to be distinguishable from the ambient temperature and salinity fields. The anomalies reduce in time under erosion by the double diffusion and the salt-finger convection, which develop along with the rotation decay, because of viscose resistance and slow mixing by the ambient turbulence. In the situation when the lens initially is fully or well enough mixed ($0 \le \sigma << 1$) the significant increase of lens horizontal size can occur during the inviscid stage and therefore the lens rotation becomes insignificant and the final decay is similar to the no rotation lens decay. Note that this approach relates to the dynamics of density intrusive lenses with small enough horizontal scales and that allows neglecting the Earth rotation.

The Mediterranean lenses have horizontal scales of several tens of kilometers and therefore the Coriolis force of the Earth rotation becomes an important component in the total balance of forces. We extend the force balance in (17)—(18) adding the radial, F_{fr}, and the azimuthal, $F_{f\varphi}$, components of the Coriolis force of the Earth rotation that is characterized by the Coriolis parameter f of the Earth rotation. The extended dynamic equations take the form

$$\rho_H \frac{d^2R}{dt^2} = F_g + F_w + F_{Cr} + F_{fr} + F_{vr}, \tag{23}$$

$$\rho_H \frac{dR\omega}{dt} = F_{C\varphi} + F_{f\varphi} + F_{v\varphi}, \tag{24}$$

where the forces F_{fr} and $F_{f\varphi}$ are

$$F_{fr} = \rho_H v_\varphi f = \rho_H R\omega f, \tag{25}$$

$$F_{f\varphi} = -\rho_H v_r f = -\rho_H \dot{R} f. \tag{26}$$

It can be seen in the equation (23) that the density heterogeneities with anti-cyclonic rotation ($\omega < 0$) have the Coriolis force of the Earth rotation as a stabilizing factor, while the cyclonic rotation ($\omega > 0$) is an additional destabilizing one. Indeed if we assume the lens to be still thick enough that the viscous terms in (23)—(24) can be neglected then there is a steady state, $\dot{R} = \dot{\omega} = 0$, with the force balance

$$F_g + F_{Cr} + F_{fr} = 0. \tag{27}$$

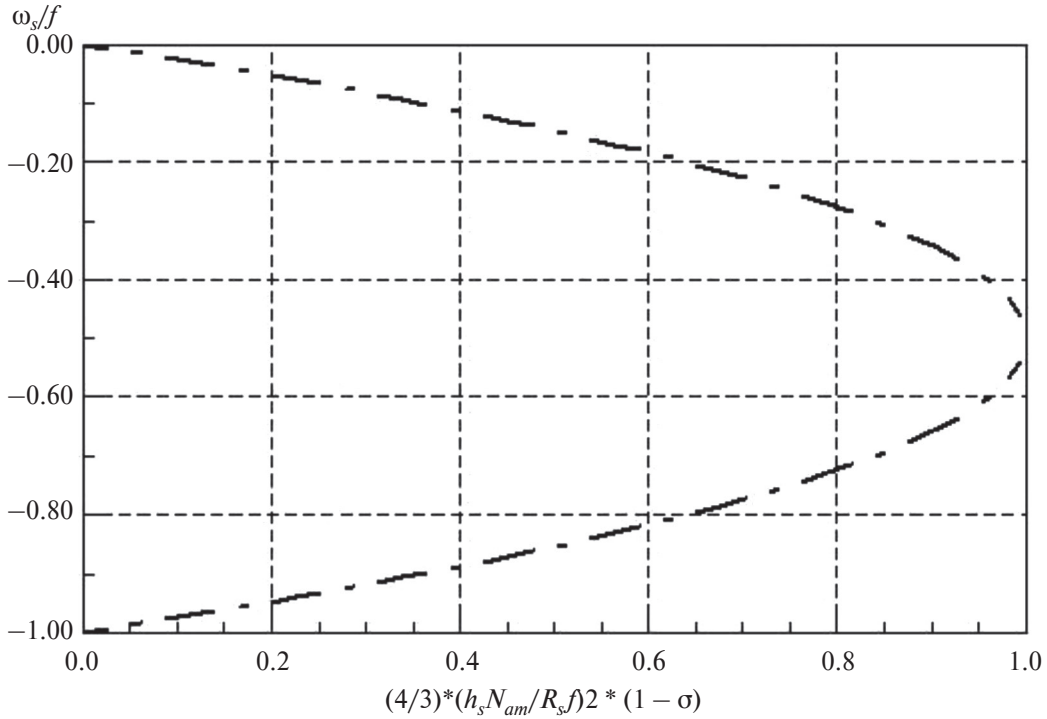

Fig. 2. The lens equilibrium angular velocity of steady rotation ω_s versus a dimensionless parameter combined of the lens equilibrium sizes, the mixing ratio and the ambient stratification: h_s — the lens equilibrium semi-thickness, R_s is the lens equilibrium radius, σ is the mixing ratio, N_{am} is the Brunt — Väisälä frequency that characterizes the ambient stratification, f is the Coriolis parameter.

The use of equations (14), (19) and (25) reduces the force balance (27) to the condition of dynamic equilibrium

$$\frac{\omega_s}{f} = -\frac{1}{2}\left(1 \pm \sqrt{1 - \frac{4(1-\sigma)}{3}\left(\frac{h_s N_{am}}{R_s f}\right)^2}\right), \quad 0 < \sigma < 1, \tag{28}$$

where index s means that the variables ω, h, and R take the equilibrium constant values $\omega = \omega_s$, $h = h_s$ and $R = R_s = \left(V / 2\pi h_s\right)^{1/2}$ because of (12). It follows from this equation that the lens angular velocity of steady rotation ω_s satisfies to the following inequality

$$-1 < \frac{\omega_s}{f} < 0 \tag{29}$$

and because of the expression under the square root sign must be positive

$$R_s f \sqrt{\frac{3}{4(1-\sigma)}} \geq h_s N_{am}. \tag{30}$$

In the case of fully mixed lens ($\sigma \to 0$) the lens semi-thickness h_s and radius R_s, due to the lens intrusion into the ambient water, have an asymptotic behavior $h_s \to 0$ or $R_s \to \infty$. Correspondingly, the asymptotic behavior of the lens angular velocity of steady rotation has two limits $\frac{\omega_s}{f} \to \left(-1 \text{ and } -0\right)$. The inequality (30) shows that the lens semi-thickness h_s must be always less than $h_{s\max} = \sqrt[3]{3Vf^2 / 8\pi(1-\sigma)N_{amb}^2} = \sqrt[3]{3h_0 f^2 / 4R_0(1-\sigma)N_{amb}^2}\,R_0$, and, correspondingly, the radius of steady rotating lens must be always greater than $R_{s\min} = \sqrt[6]{4(1-\sigma)N_{amb}^2 / 3f^2}\,(V / 2\pi)^{1/3}$. That corresponds to the case when the inequality (30) becomes an equality and then

$$\frac{h_{s\max}}{R_{s\min}} = \sqrt{\frac{\pi h_{s\max}^3}{V}} = \frac{V}{\pi R_{s\min}^3} = \frac{f}{N_{am}}\sqrt{\frac{3}{4(1-\sigma)}}. \tag{31}$$

The non-steady inviscid stage of lens dynamics obeys to the set of two equations

$$\rho_H \frac{d^2 R}{dt^2} = F_g + F_W + F_{kr} + F_{fr}, \tag{32}$$

$$\rho_H \frac{dR\omega}{dt} = F_{C\varphi} + F_{f\varphi}. \tag{33}$$

This set of equations is a reduced form of (24)—(25) if we neglect there the viscous terms F_{vr} given by the equation (16) and $F_{v\varphi}$ given by the equation (21). Substitution (14), (15), (19), (20), (25) and (26) in (32)—(33) allows to integrate (33). The integration result is the conservation law of the lens absolute angular momentum L_a that is

$$R^2\left(2\omega + f\right) = L_a = \text{const} \tag{34}$$

and then the lens angular velocity ω is

$$\omega = 0.5\left(L_a R^{-2} - f\right). \tag{35}$$

Substitution (35) into (32) reduces the equation (32) to an equation that describes the attenuated nonlinear oscillations around the steady equilibrium state (27)—(31). The analysis of small amplitude oscillations in vicinity of the equilibrium (27)—(31) shows that the oscillations occur with the lens natural frequency Ω defined by the equation

$$\Omega^2 = f^2 + 3\left(\omega_s + f\right)\omega_s + \left(h_s / R_s\right)^2\left(\frac{5}{3} - \sigma\right)N_{am}^2. \tag{36}$$

One can see that the lens stratification, the ambient stratification and the lens volume V define the natural frequency Ω. The internal wave radiation ($F_w \neq 0$) causes the degeneration of oscillations and approaching the lens dynamics to the equilibrium state (27)—(31).

The viscosity causes, equations (23)—(24), additional damping of the lens oscillations, changes the lens angular momentum and the lens energy. Then the conditions of equilibrium state change in time, and the lens dynamics shifts from fast rotation to slow rotation, and then the lens vertical size passes over its maximum. All these results relate to the lenses with anti-cyclonic rotation. The lenses with cyclonic rotation do not have an equilibrium state, they continuously change in time in the course of the non-viscous phase. Under certain conditions the cyclonic lens can re-rotate to anti-cyclonic rotation according to (35).

The developed model of the rotating intrusive lens on the rotating Earth allows characterization of the lens principal dynamical features. The evolution of a lens, which center of gravity settles down at a level of equal density, results from action of following forces: the surplus pressure due to seawater density difference between the well mixed seawater inside of the lens and the vertical distribution of the ambient density; the forces due to the intrinsic rotation of the lens, the centrifugal force, and the Coriolis' force of the Earth rotation; the resistance forces due to radiation of internal waves and the viscosity. There are two main stages of evolution of the lens:

a) Initial stage of the inviscid ("young lens") on which the balance of forces is determined by forces of inertia, pressure, centrifugal, Coriolis and the radiation of internal waves. For lenses with an anti-cyclonic rotation, the Coriolis force is a stabilizing factor, which prevents the disintegration of the lens and limits its geometrical size and rotation speed. The last are defined from a condition of balance of the superfluous pressure and the forces, centrifugal and Coriolis, and depend on initial potential energy of the lens and its initial angular momentum.

The lenses with the cyclonic rotation, to the contrary to the lenses having an anti-cyclonic rotation, are just more destabilized by the Coriolis' force, and they can reach small thicknesses during this initial stage. The degradation mechanism due to mass exchange with the ambient seawater works more efficiently for lenses with small thicknesses. Hence the lenses with cyclonic rotation should have smaller, in comparison with anti-cyclonic lenses, vertical size and less distinguishable by the anomalies of hydro-physical and hydro-chemical characteristics.

b) The final viscous stage ("old lens") is characterized by the slow decrease of the lens vertical size $2h$ up to its limiting value, which depends on the initial size of the lens, its initial stratification and the stratification of ambient seawater. In the course of the viscous stage the exchange with the ambient water by heat, salt and any other admixtures may affect significantly on the lens anomalies degradation with degradation characteristic temporal scale of about ~1 year. The lens has a slow anti-cyclonic rotation supported by the Coriolis' force.

The conservation of the lens angular momentum and its total energy play important role during the initial stage when the viscosity does not affect the lens dynamics. The lenses with anti-cyclonic rotation oscillate around the equilibrium state (27)—(31) which is characterized by the lens equilibrium geometrical sizes and the lens equilibrium angular velocity of rotation. The frequency of oscillations depends on the ambient conditions, the Coriolis' parameter,

the stratification inside the lens and the lens angular momentum. The amplitude of the oscillations is defined by the lens initial energy. The nonlinear oscillations are asymmetrical around the equilibrium state and have the oscillation period of the order of magnitude of about 10 hours. The numerical experiment duration corresponds to the temporal period of 17 hours. In the course of attenuation of the oscillations due to the radiation of internal waves the lens tends to take its equilibrium state.

In this stage the influence of viscosity causes slow reduction of the lens energy and the angular momentum. As an outcome the angular velocity of lens equilibrium rotation, the equilibrium frequency of oscillations and additional changes of the oscillation amplitude occur due to these changes of the lens energy and the angular momentum. If the anti-cyclonic lenses rotate fast ($\omega < -0.5f$) at the initial moments of time, then there is enhancement of the lens oscillations in the course of approaching of the angular velocity of lens equilibrium rotation to the value $-0.5f$, and it is accompanied by increase of the lens equilibrium thickness. When the angular velocity of lens rotation has passed the value $-0.5f$, there are monotonic decrease of the lens equilibrium thickness, the lens equilibrium angular velocity and the amplitudes of the lens oscillations. To the contrary, the lenses with cyclonic rotation are even more destabilized by the Coriolis' force and are able to reach small thicknesses during this stage. As the lens thickness is small enough then the mechanisms of lens density anomaly degradation work more efficiently by the mass and heat exchange with the ambient water. Therefore, the lenses with cyclonic rotation are expected to have smaller vertical size and less manifested by the anomalies in hydro-physical and hydro-chemical fields in comparison with anti-cyclonic lenses.

4. Results of numerical experiments

The set of model equations (32)—(33) has been solved numerically using second order the Runge-Kutta method. A lens with a volume of 1380 km^3 and a horizontal size of 62.2 km has been taken for an analysis of the model sensitivity to variations of its internal parameters and the external conditions/parameters. The lens characteristics in final experiments have been taken as 1260 km^3 of the lens volume and 56 km of the horizontal size [41]. Some simulations with different horizontal sizes for the same volume have also been carried out. Using the variations of the sizes of lenses, the internal parameters of the model and the characteristic temporal scale of lens, the all stages of the lens evolution have been studied. The ambient hydrophysical conditions had been selected from [41]. The mean density at the depth of the maximum inversion of the salinity and temperature is 1027.62 kg/m^3, ambient gradient of density $d\rho_{amb}/dz = 0.0006$ kg/m^4, its internal gradient $d\rho_I / dz = 0.0001$ kg/m^4. The basic variables of the lens dynamics, — the lens radius R, the lens semi-thickness h and the lens angular velocity ω, had been numerically analyzed. The discussion of the numerical experiments is presented below and given in fig. 3–9. The lens dynamics equations (32)—(33) includes two dissipative mechanisms: the radiation of internal wave energy and the dissipation due to viscosity. The efficiency of dissipative mechanisms has been studied varying the values of the internal parameters of the model: the internal wave radiation coefficient (k_w) and the viscosity coefficient (k_v).

If the dissipative losses are neglected ($k_w = k_v = 0$) then the solution of the system is forced oscillations with a period of 16–17 hours. Variations of amplitudes of h and ω depend on initial value of the lens angular velocity $\omega(0) = \omega_0$. If there is only the dissipative energy loss due to the internal wave radiation caused by the lens intrusion ($k_w \neq 0$, $k_v = 0$), then, starting from a certain time moment, which depends on the numerical value of k_w, the oscillations of h and ω decay and tend to take their equilibrium constant values h_s and ω_s of (27)–(31). In the case of only the viscous dissipation contributes into the dissipative losses ($k_w = 0$, $k_v \neq 0$), the lens as a temperature-salinity anomaly disappears gradually ($h \to h_{cr}$, $\omega \to 0$). In that case the temporal evolution of the lens is determined by values of ω_0 and the viscous internal parameter k_v. Numerical examples below demonstrate behavior of the lens in these regimes quantitatively.

Fig. 3, *a*, *b* shows the case of temporal variability of the non-dissipative system ($k_w = k_v = 0$): the lens semi-thickness $h(t)$, shown in fig. 3, *a*, and the lens angular velocity $\omega(t)$, shown in fig. 3, *b*, are given for different initial angular velocities of lens rotation ω_0:

$\omega_0 = 0$ (curve (3) in fig. 3, *a*), the range of oscillations around $h_s \approx 224$ m is 7.45 m that constitutes about 0.03 of h_s and therefore they are invisible; the period of these oscillations is 17.5 hours;

$\omega_0 / f = -1.5$, 0.5, these oscillations coincide and are given in fig. 3, *a* by the curve (2), they have the same period as in the previous case with $\omega_0 / f = 0$ but have more significant range of oscillations that is 172 m (228 m $\gtrsim h \gtrsim$56 m) around the semi-thickness $h_s \approx 113$ m;

$\omega_0 = -0.5f$ (curve (1) in fig. 3, *a*), the semi-thickness $h(t)$ oscillates around the constant semi-thickness equilibrium value $h_s \approx 672$ m, the oscillation range is 1283 m (1511 m $\gtrsim h \gtrsim$ 228 m) and the oscillation period is about 16.5 hour;

the oscillations of the semi-thickness $h(t)$ around its equilibrium values h_s are nonsymmetrical (with exceptions of the case $\omega_0 = 0$): the amplitude of $h(t)$ is greater in the half-periods where h is greater than 228.22 m; in our case $h > 673$ m for $\omega_0 = -0.5f$ and $h < 114$ m for $\omega_0 = -1.5f$, $+0.5f$;

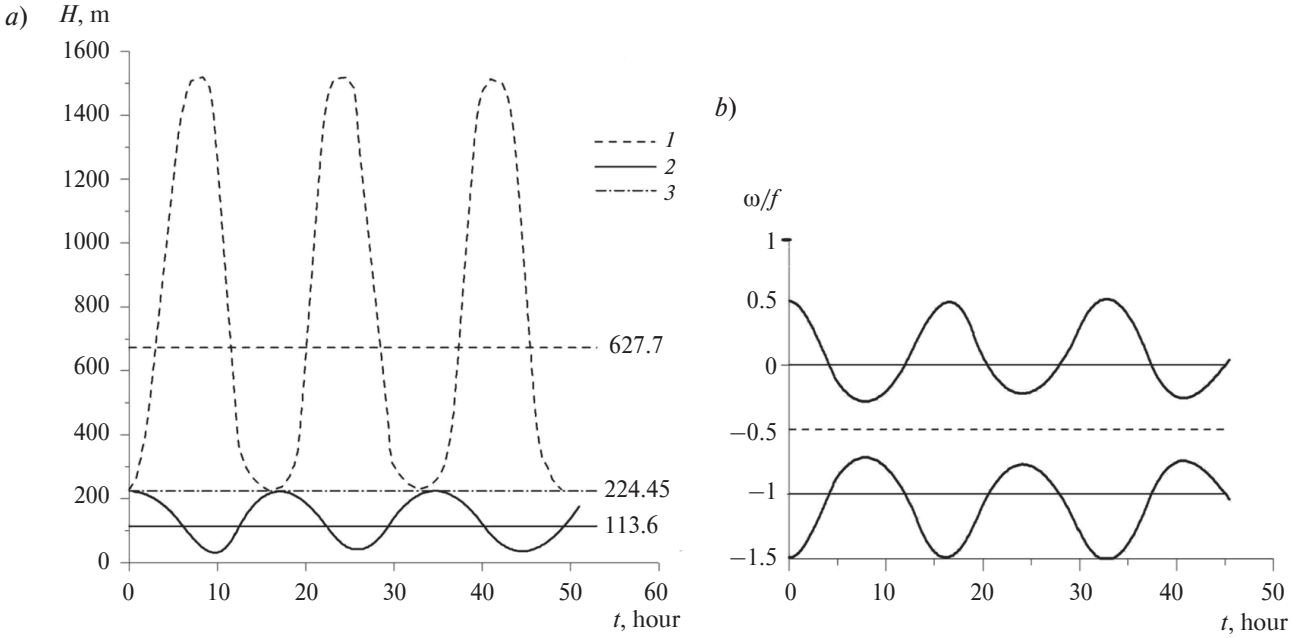

Fig. 3. The lens forced oscillations with absence of the dissipative losses ($k_w = k_v = 0$) for different values of the initial angular velocities of rotation ω_0: *1* — $\omega_0 = -0.5f$, $\omega_0 = 0.5f$; *2* — $\omega_0 = -1.5f$; *3* — $\omega_0 = 0$; *a* — temporal evolution of the lens semi-thickness $h(t)$; *b* — temporal evolution of the angular velocities of the lens rotation $\omega(t)$, ($f = 0.727*10^{-4}\text{s}^{-1}$). The horizontal lines in (3*a*) and (3*b*) correspond to the equilibrium values of h and ω for $k_w \neq 0$

the numerical solutions of the lens angular velocity $\omega(t)$ in fig. 3, *b* are calculated for $\omega_0 = 0$ and $\omega_0 = -0.5f$ which correspond to the straight lines that are parallel to abscissa axis, and the oscillating solutions for $\omega_0 = -1.5f$, $0.5f$ which are symmetrical relatively $\omega_0 = -0.5f$ with the range of $0.75f$ and the period of about 17.5 hour.

The influence of the initial value of the angular velocity $\omega(0) = \omega_0$ on the lens semi-thickness $h(t)$ and the angular velocity $\omega(t)$ is shown in fig. 4, *a*, *b*; the curve 3 demonstrates the equilibrium semi-thickness h_s (fig. 4, *a*) and the equilibrium angular velocity ω_s (fig. 4, *b*) versus ω_0 in the inviscid lens dynamics case ($k_w \neq 0$, k_v=0); the solution for the lens semi-thickness h is symmetrical relatively the straight line ($-0.5f$, h); three intervals are well pronounced in fig. 4, *a*, *b*:

h-Interval (I): $-1.5f \leq \omega_0 \leq -f$. The maximal values $h_{\max}$, (curve 1), of the amplitudes of forced oscillations of $h(t)$ are constant $h_{\max} = h_{\max|\omega 0=0}$ for all values ω_0 of this interval, while the minimal values $h_{\min} \to 0$, (curve 2), and the lens equilibrium thickness $h_s \to h_{crit}$, (curve 3). The period of the lens semi-thickness oscillations $h(t)$ is 17.5 hour.

h-Interval (II): $-f < \omega_0 < 0$. In this range of ω_0 the curve 2 of the minimal amplitude $h_{\min}$ of the lens semi-thickness oscillations $h(t)$ is a constant that coincides with $h_{\max|\omega 0=0} \approx 228$ m. The maximal amplitude $h_{\max}$ of the lens semi-thickness oscillations $h(t)$, curve 1 in fig. 4, *a*, has the maximal value of $h_{\max} = 1511$ m at the initial value of the angular velocity $\omega(0) = \omega_0 = -0.5f$, and after that $h_{\max}$ decreases to the value of $h_{\max|\omega 0=-f} = h_{\max|\omega 0=0} \approx 228$ m. The lens equilibrium thickness h_s versus ω_0, curve 3, has a similar form with the maximal value $h_s(-0.5f) = h_{s\max} = 674$ m and $h_s(-f) = h_s(0) = h_{\max|\omega 0=-f} = h_{\max|\omega 0=0} \approx 228$ m. Also, in this range of the initial value of the angular velocity ω_0 the maximal amplitudes $h_{\max}$, (curve 1), and the minimal amplitudes $h_{\min}$, (curve 2), of the lens semi-thickness oscillations $h(t)$ are symmetrical relatively the initial value of the angular velocity $\omega_0 = -0.5f$. The period of the lens semi-thickness oscillations $h(t)$ is 16.5 hour.

h-Interval (III): $0 < \omega_0 < f$. In this range of ω_0 the lens semi-thickness $h(t)$ oscillates around the equilibrium semi-thickness h_s with the period of about 17.5 hour. The maximal amplitude $h_{\max}$ of the lens semi-thickness oscillations $h(t)$ is a constant that is $h_{\max} = h_{\max|\omega 0=0} = 228.22$ m. The minimal amplitude $h_{\min}$ of the lens semi-thickness oscillations $h(t)$ and the equilibrium semi-thickness h_s tend to zero, $h_{\min} \to 0$, $h_s \to 0$.

The maximal amplitudes $h_{\max}$ of the lens semi-thickness oscillations $h(t)$ in the h-Intervals (I) and (III) of the initial values ω_0 coincide with the minimal amplitudes $h_{\min}$ of the oscillations $h(t)$ of the h-Interval (II), and they correspondingly are $h_{\max} = h_{\min} = 228.22$ m. The period of h-oscillation in the h-Interval (II) is 16.5 hour that is one an hour less than the periods of h-oscillation in the h-Intervals (I) and (III), 17.5 hour. The amplitude $h_{\min}$ of the lens semi-thickness oscillations $h(t)$, curve 3, becomes less than h_{crit}, curve 4, when the initial values of the lens angular velocity $\omega_0 \leq -1.75f$ or $\omega_0 \geq 0.75f$. Therefore we may assume that the numerical values $\omega_0 = -1.75f$ and $\omega_0 = 0.75f$ can be taken as the lower and upper limits of the possible initial values of the lens angular velocity ω_0 in this approach.

Also, we can make a physical interpretation: the initially fast rotating lens, $\omega_0 \le -1.75f$ or $\omega_0 \ge 0.75f$, may be unstable and may break up to several stable lens-like structures as it was observed in field measurements [7, 38] and shown in fig. 1.

The influence of the initial values $\omega(0) = \omega_0$ on the angular velocity of lens rotation $\omega(t)$ is shown in fig. 4, *b*. The total range of the initial values ω_0, $-1.5f \le \omega_0 \ge f$, is the same as in fig. 4, *a*. The three ranges of the initial values $\omega(0) = \omega_0$ in fig. 4, *a* are well pronounced in the plots of the characteristics of angular velocity of lens rotation ω_{max}, ω_{min} and ω_s in fig. 4, *b*:

ω-Interval (I): $-1.5f \le \omega_0 \le -f$. The numerical values of the characteristics ω_{max}, ω_{min} and ω_s correspondingly are as $-0.75f \le \omega_{max} \le -f$, $-1.5f \le \omega_{min} = \omega_0 \le -f$ and $\omega_s = -f$; $\omega_s = -f$.

ω-Interval (II*a*): $-f \le \omega_0 \le -0.5f$. The numerical values of the characteristics ω_{max}, ω_{min} and ω_s correspondingly are: $-f \le \omega_{max} = \omega_0 \le -0.5f$; $-f \ge \omega_{min} \ge \omega_{min}$ $(\omega_0 = -0.75f) = -1.25f$ and ω_{min} $(\omega_0 = -0.75f) = -1.25f \le \omega_{min} \le -0.5f$ because $\omega_{min} = -1.25f$ is the minimal numerical value of ω_{min} at the point $\omega_0 = -0.75f$ of this interval; $-f \le \omega_s \le -0.5f$.

ω-Interval (II*b*): $-0.5f \le \omega_0 \le 0$. The numerical values of the characteristics ω_{max}, ω_{min} and ω_s correspondingly are: $-0.5f \le \omega_{max} \le \omega_{max}$ $(\omega_0 = -0.25f) = 0.25f$ and ω_{max} $(\omega_0 = -0.25f) = 0.25f \ge \omega_{max} \ge 0$ because $\omega_{min} = 0.25f$ is the maximal numerical value of ω_{max} at the point $\omega_0 = -0.25f$ of this interval; $-0.5f \le \omega_{min} = \omega_0 \le 0$; $-0.5f \le \omega_s \le 0$.

ω-Interval (III): $0 \le \omega_0 \le 1.5f$. The numerical values of the characteristics ω_{max}, ω_{min} and ω_s correspondingly are: $0 \le \omega_{max} = \omega_0$; $0 \le \omega_{min} \ge -0.25f$; $\omega_s = 0$.

The initial values $\omega(0) = \omega_0$ of the range $[-1.5f, 1.5f]$ cause significant variations the characteristics of angular velocity of lens rotation ω_{max}, ω_{min} and ω_s which can be taken as $[-1.5f \leqslant h_{max} = h_{min} = h_s \leqslant 1.5f]$ that follows of fig. 4, *b*. The equilibrium values ω_s are equal to zero all over of the range ω-Interval (III). The lens rotation angular velocity ω does not oscillate at three initial values ω_0 ($\omega_0 = -f$, $\omega_0 = -0.5f$ and $\omega_0 = 0$) where $\omega_{max} = \omega_{min} = \omega_s$. However, the lens semi-thickness does not oscillate at two initial values ω_0 ($\omega_0 = -f$ and $\omega_0 = 0$) where $h_{max} = h_{min} = h_s$. Also, the angular velocity ω has its equilibrium values ω_s as constants in ω-Interval (I) and ω-Interval (III) of the ranges of initial values of ω_0.

The results of numerical experiments shown in fig. 4, *a*, *b* allow a conclusion that the current Meddie's state, characterized by the measured quantities h_{max}, h_{min}, ω_{max} and ω_{min}, may provide a qualitative information on the lens three important dynamics characteristics h_s, ω_s, ω_0.

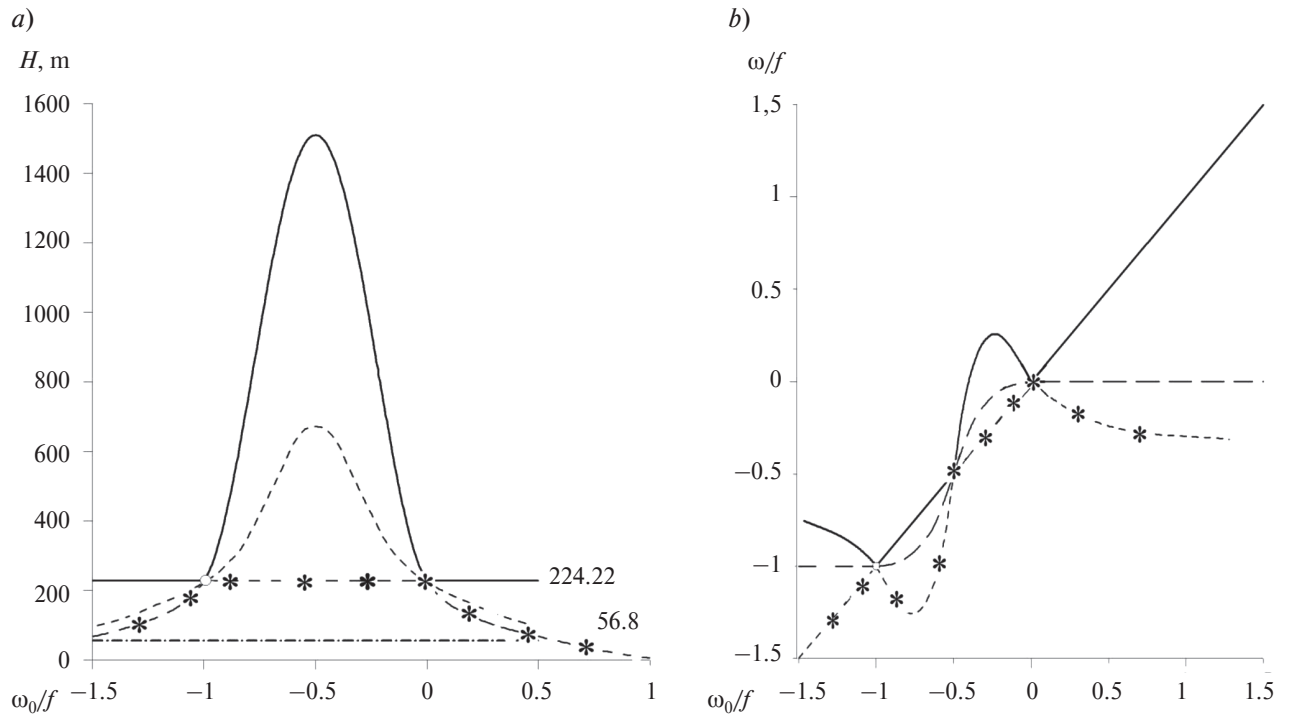

Fig. 4. The amplitudes of forced oscillations of (*a*) the lens semi-thickness *h* and (*b*) the lens angular velocities of rotation ω versus of the lens initial angular velocities of rotation ω_0. The legends of figures correspondingly are: $H = (h_{min}, h_{max}, h_s, h_{crit})$, $\omega = (\omega_{min}, \omega_{max}, \omega_s)$, (——1) — maximal values, (–*–*– 2) — minimal values, (– — - — 3) — equilibrium values, (–×–×–×– 4) — h_{crit} in fig. 4, *a*.

The numerical experiments of the inviscid ($k_\nu = 0$) lens dynamics with two different values of the internal wave radiation coefficient k_w ($k_w = 0.1$, 1) are presented in the form of the characteristic time of the equilibrium regime adjustment $\boldsymbol{T}$ versus the initial angular velocity of lens rotation ω_0 in fig. 5. The minimal characteristic timescales values $\boldsymbol{T}$ correspondingly are $\boldsymbol{T} = 80$ hours ($k_w = 1$) and $\boldsymbol{T} = 800$ hours ($k_w = 0.1$) both at $\omega_0 = -0.5f$. The $\boldsymbol{T}_1$ (ω_0, $k_w = 1$) and $\boldsymbol{T}_2$ (ω_0, $k_w = 0.1$) are almost symmetrical relatively the point of the initial angular velocity of lens rotation $\omega_0 = -0.5f$. The initially fast rotating lenses $\omega_0 = -1.5f$ and $\omega_0 = f$ have the longer characteristic time of the equilibrium regime adjustment $\boldsymbol{T}$ than at $\omega_0 = -0.5f$ that can be shown as an inequality chain: $\boldsymbol{T}_2(f, 0.1) \gtrsim \boldsymbol{T}_2(-1.5f, 0.1) \gtrsim \boldsymbol{T}_1(f, 1) \gtrsim \gtrsim \boldsymbol{T}_1(-1.5f, 1) > > \boldsymbol{T}_2(-0.5f, 0.1) > \boldsymbol{T}_1(-0.5f, 1)$. Hence, the outcome of the strong wave resistance ($k_w = 1$) in the course of the lens intrusion into the ambient water is the short characteristic time of the equilibrium regime adjustment $\boldsymbol{T}$.

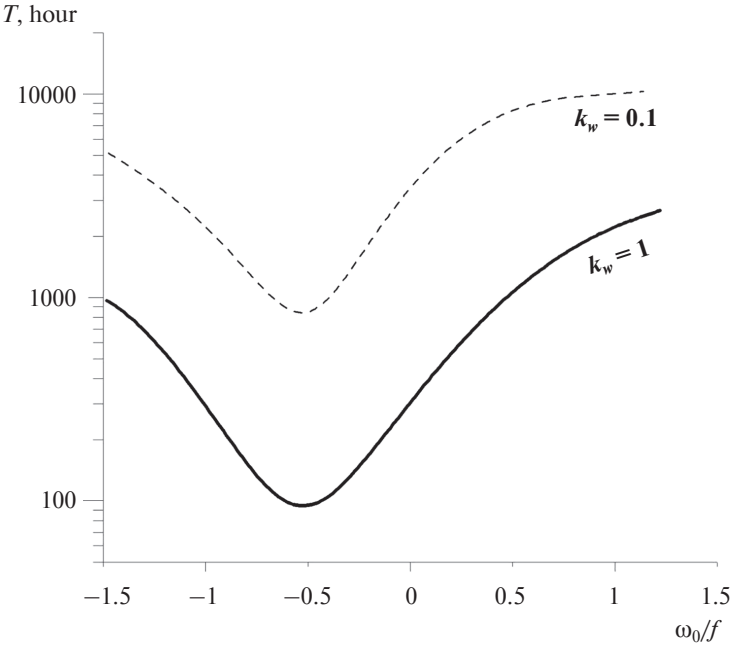

Fig. 5. The temporal adjustment scale $\boldsymbol{T}$ to the equilibrium state (27)—(31) versus the lens initial angular velocities rotation $\omega(0) = \omega_0$ for different values of the internal wave radiation coefficient k_w in the case of the lens inviscid ($k_\nu = 0$) dynamics case.

The temporal evolution of lens semi-thickness h in cases with different numerical values of the effective viscosity coefficient ($k_\nu = 0.1$, $k_\nu = 1$) and zero the internal wave radiation ($k_w = 0$) are shown in fig. 6, *a*, *b* where the H-coordinate represents the lens characteristics H = (h, the upper branch — $h_{\max}$, the lower branch — $h_{\min}$). The curves 1–3 in fig. 6, *a* and the curves in fig. 6, *b* correspond to the different values of lens initial angular velocity ω_0: *a*) curve 1: $\omega_0 = -0.75f$, curve 2: $\omega_0 = -0.25f$, curve 3: $\omega_0 = 0.25f$; *b*) $\omega_0 = -0.5f$.

In the numerical experiment with the lens initial angular velocity $\omega_0 = 0$ the lens semi-thickness $h(t)$ oscillates around h_s, the swing amplitude $h_{\max} - h_{\min}$ of the lens oscillation becomes $h_{\max} - h_{\min} = 0$ with time t growth, that is a certain time moment t when the oscillation of lens semi-thickness ends and $h_{\max} = h_{\min} = h_s$, and finally $h(t)$ approaches to the value of h_{crit} which is $h_{crit} = \sigma\, h(0) \approx 38$ m for the lens with $V = 1380$ km^3 where the initial value $h(0) = 228$ m and the lens mixing parameter $\sigma = 1.666$. The numerical experiments shown in fig. 6, *a* have been carried out for the lens with the initial values of the lens angular velocity ω_0 of the range $-0.75f \le \omega_0 \le 0.25f$. The $h_{\max}$ (the upper branch of the curve 1, $\omega_0 = -0.75f$) increases from the initial value $h_{\max}(0) = h(0) \approx 228$ m to its largest value $h_{\max}$ (4 *day*) ≈ 1000 m, and $h_{\min}$ (the lower branch of the curve 1, $\omega_0 = -0.75f$) increases from the initial value $h_{\min}(0) = h(0) \approx 228$ m to its largest value $h_{\min}$(30 day) ≈ 500 m, and the largest value of the lens swing amplitude $h_{\max}$(4 day) − $h_{\min}$(*4 day*) ≈ 600 m. The lens oscillation ends when $h_{\max}$(50 day) = $h_{\min}$(50 day) = $h_s \approx 475$ m. After that the lens semi-thickness $h(t)$ decreases approaching to the critical semi-thickness value h_{crit} at the time $t \approx 1000$ day. The numerical experiment with the same initial angular velocity $\omega_0 = -0.75f$ but with the effective viscosity coefficient $k_\nu = 0.1$ is shown in fig. 6, *a* by the dashed curve 1. This case is qualitatively similar to the previous experiment with $k_\nu = 1$ (fig. 6, *a*, the solid curve 1) but has quantitative differences: the largest value $h_{\max}$ (10 day) ≈ 900 m, the largest value $h_{\min}$ (120 day) ≈ 550 m, and the largest value of the lens swing amplitude $h_{\max}$(10 day) − $h_{\min}$(10 day) ≈ ≈ 600 m; the end of the lens oscillation at $h_{\max}$(300 day) = $h_{\min}$(300 day) = $h_s \approx 540$ m; the lens semi-thickness $h(t)$ takes the critical semi-thickness value h_{crit} at the time $t \approx 4000$ day. The results of numerical experiments with the lens initial angular velocity $\omega_0 = -0.5f$ are shown in fig. 6, *b* by the dashed curve for the effective viscosity coefficient $k_\nu = 0.1$ and by the solid curve for $k_\nu = 1$. In the case of $\omega_0 = -0.5f$ and $k_\nu = 1.0$, the maximal amplitude of oscillations $h_{\max}$ (the upper branch of the solid curve) increases from $h_{\max}(0) = h(0) = 232$ m to $h_{\max}$(0.2 day) = 1212 m and after that $h_{\max}$ decreases to $h_{\max}$(12 day) = $h_s \approx 500$ m, the minimal amplitude of oscillations $h_{\min}$ (the lower branch of the solid curve) increases from $h_{\min}(0) = h(0) = 232$ m to $h_{\min}$(0.2 day) = 255 m and after that $h_{\min}$ increases to $h_{\min}$(12 *day*) = $h_s \approx 500$ m, the largest value of the lens swing amplitude $h_{\max}$(0.2 day) − $h_{\min}$(0.2 day) ≈ 957 m, at the time moment $t = 12$ day the swing amplitude $h_{\max}$(12 day) − $h_{\min}$(12 day) = 0 that is the oscillation of lens semi-thickness ends at the time moment $t \approx 12$ day. The same case of $\omega_0 = -0.5f$ with the effective viscosity coefficient $k_\nu = 0.1$ is shown in fig. 6, *b* by the dashed curve. The maximal amplitude of oscillations $h_{\max}$ (upper branch of the dashed curve)

increases from $h_{max}(0) = h(0) = 232$ m to $h_{max}(0.2\ day) = 1517$ m and after that h_{max} decreases to $h_{max}(35\ day) = h_s \approx$ ≈ 500 m, the minimal amplitude of oscillations h_{min} (lower branch of the dashed curve) increases from $h_{min}(0) =$ $= h(0) = 232$ m to $h_{min}(0.2\ day) = 249$ m, the largest value of the lens swing amplitude $h_{max}(0.2\ day) - h_{min}(0.2\ day) \approx$ ≈ 1268 m and after that h_{min} increases to $h_{min}(35\ day) = h_s \approx 500$ m, at the time moment $t = 35$ day the swing amplitude $h_{max}(35\ day) - h_{min}(35\ day) = 0$ that is the oscillation of lens semi-thickness ends at the time moment $t \approx$ ≈ 35 day. The results of numerical experiments with the initial values $\omega_0 = -0.25f$ and the effective viscosity coefficient $k_v = 0.1$ (the dashed curve 2 in fig. 6, *a*) and $k_v = 1.0$ (the solid curve 2 in fig. 6, *a*) have the similar behavior as in the case $\omega_0 = -0.5f$ in fig. 6, *b* but differs in quantitative manner: $k_v = 0.1$, largest $h_{max}(0.2\ day) \approx 670$ m; $k_v = 1$, largest $h_{max}(0.2\ day) \approx 621$ m; $k_v = 0.1$, $h_{min}(0.2\ day) \approx 218$ m; $k_v = 1$, $h_{min}(0.2\ day) \approx 218$ m; $k_v = 0.1$, the largest value of the lens swing amplitude $h_{max}(0.2\ day) - h_{min}(0.2\ day) \approx 452$ m; $k_v = 1$, the largest value of the lens swing amplitude $h_{max}(0.2\ day) - h_{min}(0.2\ day) \approx 403$ m; $k_v = 0.1$, at $t = 60$ day the swing amplitude $h_{max}(60\ day) - h_{min}(60\ day) = 0$ and $h_{max}(60\ day) = h_{min}(60\ day) = h_s \approx 316$ m; $k_v = 1$, at $t = 12$ day the swing amplitude $h_{max}(12\ day) - h_{min}(12\ day) = 0$ and $h_{max}(12\ day) = h_{min}(12\ day) = h_s \approx 330$ m; the lens lifetime $h(t_{lf}) = h_{crit}$ for $k_v = 0.1$, $k_v = 1$, $t_{lf} = 1000$ day. The lens temporal variability of the case $\omega_0 = 0.25f$ is similar to the case $\omega_0 = -0.25f$ but is significantly weaker: $k_v = 0.1$, largest $h_{max}(0.2\ day) \approx 207$ m, $h_{min}(0.2\ day) \approx 88$ m, the largest swing amplitude $h_{max}(0.2\ day) - h_{min}(0.2\ day) = 119$ m and at the end of the lens oscillatory lifetime $h_{max}(22\ day) = h_{min}(22\ day) = h_s \approx 316$ m; $k_v = 1$, largest $h_{max}(0.2\ day) \approx$ ≈ 203 m, $h_{min}(0.2\ day) \approx 105$ m, the largest swing amplitude $h_{max}(0.2\ day) - h_{min}(0.2\ day) = 98$ m and at the end of the lens oscillatory lifetime $h_{max}(10\ day) = h_{min}(10\ day) = h_s \approx 316$ m; the lens lifetime $h(t_{lf}) = h_{crit}$ for $k_v = 0.1$, $k_v = 1$, $t_{lf} \approx 1000$ day. The set of numerical experiments presented in fig. 6, *a*, *b* well demonstrates the phase of the "young" lens dynamics accompanied by intensive nonlinear oscillations of the lens geometrical sizes and the angular velocity of lens rotation. The end of the lens oscillation varies from 10 day to 300 day. The largest swing amplitude varies from $h_{max} - h_{min} \approx 98$ m to $h_{max} - h_{min} \approx 600$ m.

The lens lifetime t_{lf}, including the duration of the phase of the "young" lens dynamics, varies from 1000 day to 4000 day, and hence the temporal phase duration of the "mature" lens dynamics has the same order of magnitude as t_{lf} considering the temporal phase of the "young" lens dynamics duration which does not contribute much into t_{lf}. The temporal variability of lens dynamics is mostly affected by the initial value the lens rotation angular velocity ω_0 while the influence of the effective viscosity coefficient k_v is notably less.

Figure 7 shows the influence of the ambient stratification on the lens oscillatory regime in the numerical experiments with the initial angular velocity $\omega_0 = 0$, the internal wave radiation coefficient $k_w = 0$ and the effective viscosity coefficient $k_v = 0$. In this set of numerical experiments the ambient density gradient $(d\rho/dz)_{amb}$ varies in the range from 10^{-4} kg/m^4 to $5 \times$ $\times 10^2$ kg/m^4, the upper limit here has been chosen for simulating well mixed condition inside the lens under the condition that

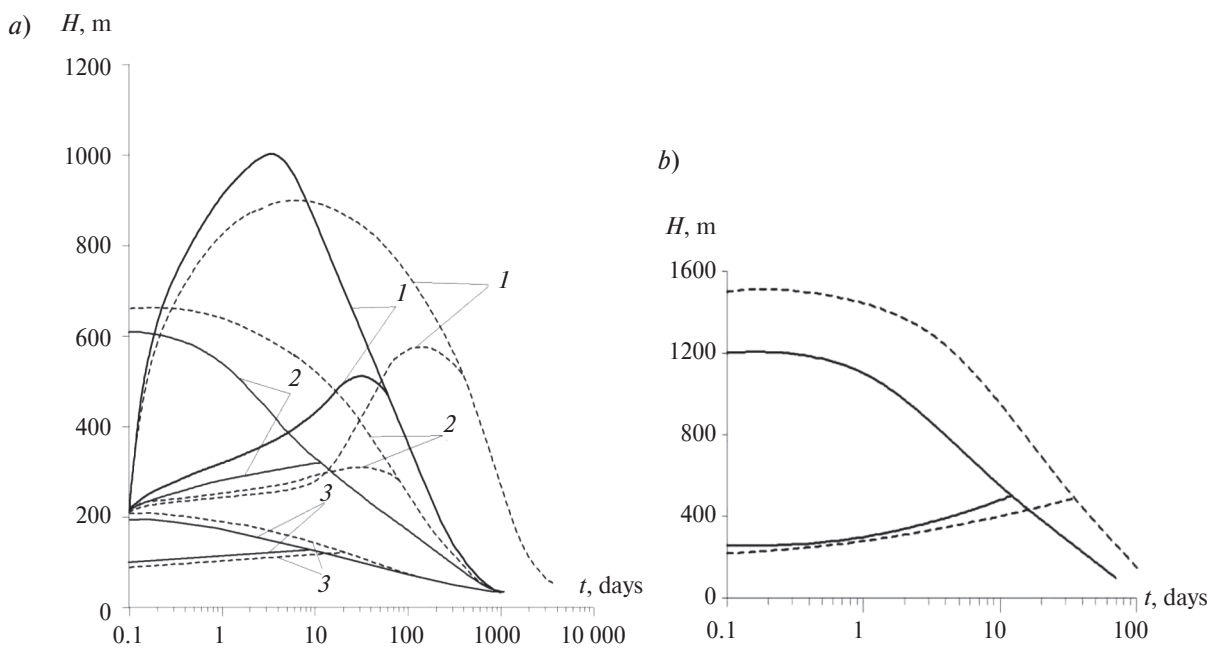

Fig. 6. Temporal evolution of semi-thickness h in the case of absence of internal wave radiation ($k_w = 0$). The legends of figures correspondingly are: $H = (h$, upper branch — h_{max}, lower branch — $h_{min})$; (—) — $k_v = 1$, (––) — $k_v = 0.1$; *a*) *1* — $\omega_0 = -0.75f$, *2* — $\omega_0 = -0.25f$, *3* — $\omega_0 = 0.25f$; *b*) $\omega_0 = 0.5f$.

the density gradient inside the lens does not change. The lens minimal semi-thickness h_{min} decreases from $h_{min} = h_{max} = h(0) \approx 228$ m to $h_{min} = 0$ with the increase of the ambient density gradient $(d\rho/dz)_{amb}$ from 10^{-4} kg/m^4 to 1 kg/m^4 that corresponds to the variation of the mixing parameter σ in the range $1 > \sigma > 10^{-4}$. The minimal angular velocity of lens rotation ω_{min} tends to the value $\omega_{min} \to -0.5f$. The maximal amplitudes h_{max} and ω_{max} coincide with the maximal amplitudes h_{max} and ω_{max} of the numerical experiment with the ambient density gradient $(d\rho/dz)_{amb} = 6 \times 10^{-4}$ kg/m^4. Hence the increase of the ambient density gradient $(d\rho/dz)_{amb}$ causes a decrease of the lens minimal semi-thickness h_{min} and an increase of the minimal angular velocity of lens rotation — ω_{min}. The discussed here results are analogical to the results obtained in the numerical experiments given in fig. 4, *a*, *b*.

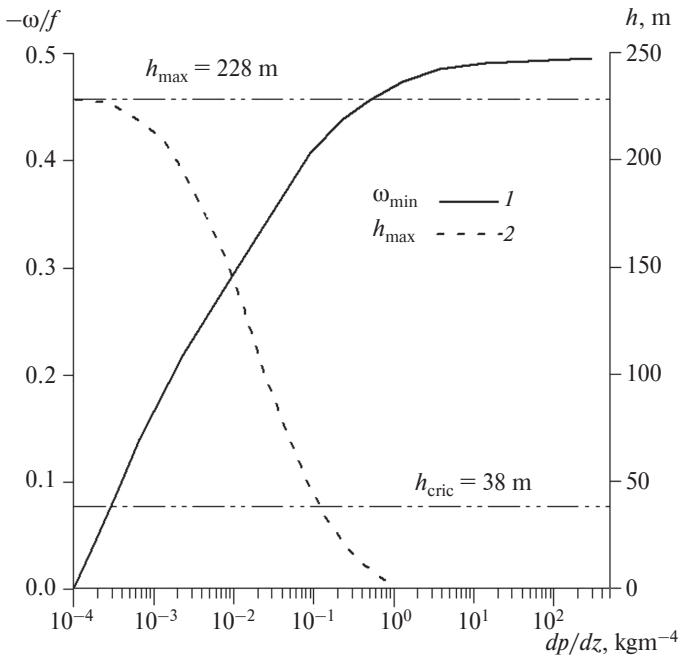

Fig. 7. The influence of the ambient density gradient $d\rho/dz_{amb}$ on the amplitudes of forced oscillations of the lens rotation angular velocity ω_{min} and the lens semi-thickness h_{max} for the lens density gradient $d\rho/dz_1 = 10^{-4}$ kg/m^4.

Figure 8 shows the numerical experiments with the full set of the forces causing the lens temporal variability. The numerical examples of lens temporal evolution are carried out for the case with the initial angular velocity $\omega_0 = -0.75f$, the initial thickness $h(0) \approx 242$ m and the initial radius $R \approx 29$ km, that corresponds to the lens volume $V \approx 1260$ km^3. The internal wave radiation coefficient is taken as $k_w = 1$. The effective viscosity coefficient is taken as $k_v = 0.01$ (keeping the order of magnitude of the molecular viscosity), $k_v = 0.1$ (keeping the order of magnitude of an intermediate viscosity) and $k_v = 1$ (keeping the order of magnitude of the turbulent viscosity). All three curves show two the well distinguishable temporal phases: the initial phase characterized by growing in time the lens semi-thickness $h(t)$ up to its largest value due to decreasing the lens anti-cyclonic angular rotation velocity from $-\omega_0 = 0.75f$ down to $-\omega = 0.5f$ caused by the viscosity influence; the concluding phase characterized by the "exponential" decaying of the lens semi-thickness $h(t)$ from its largest value at the end of the initial phase to the final thickness $h_{crit} \approx 43$ m due to the lens intrusion into the ambient

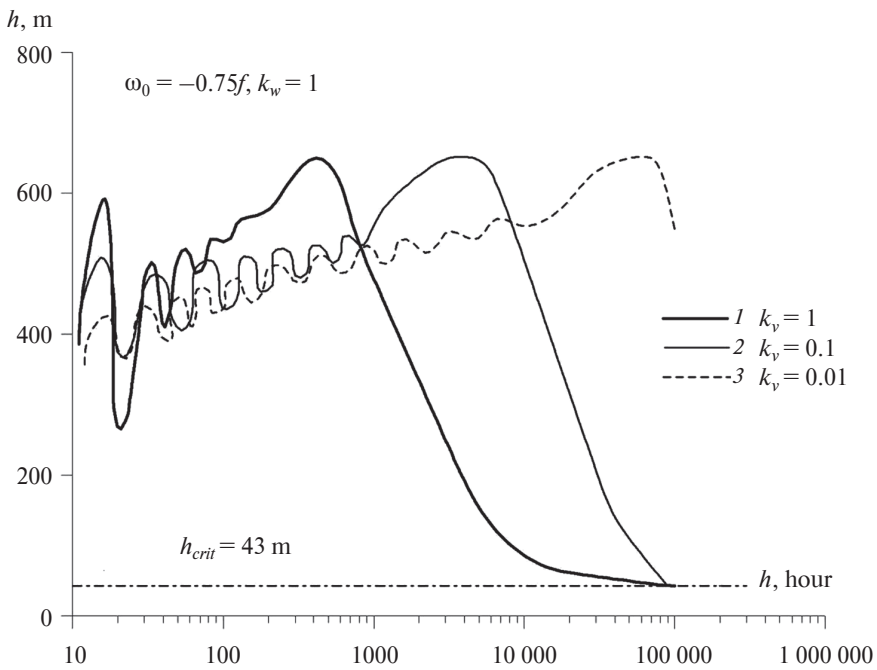

Fig. 8. Temporal variations of the lens semi-thickness $h(t)$ with different numerical values of the effective viscosity coefficient k_v.

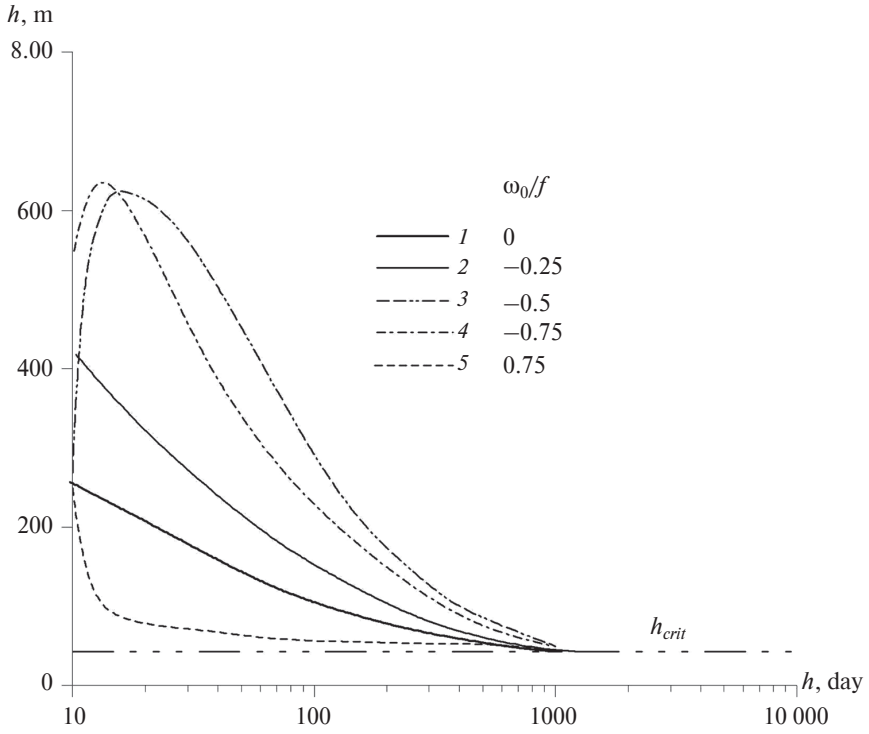

Fig. 9. The influence the initial values of the lens rotation angular velocity ω_0 on temporal variability of the lens semi-thickness $h(t)$ under the condition $k_w = k_v = 1$.

water and equalization the lens density stratification with the ambient water stratification (see also fig. 6, *a*). During the initial phase the lens semi-thickness $h(t)$ has the forced oscillations of large amplitudes. This phase duration is about 4 week for $k_v = 1$, about 8 month for $k_v = 0.1$ and about 8 year for $k_v = 0.01$. The duration of the concluding phase is about 4 year for $k_v = 1$, about 11 year for $k_v = 0.1$ and significantly longer for $k_v = 0.01$.

The results of the final experiment given in fig. 9 show the influence of the lens initial angular velocity ω_0 on the lens dynamics in the case when the internal wave radiation coefficient k_w and the effective viscosity coefficient k_v are taken as $k_w = k_v = 1$. The lens semi-thickness $h(t)$ in the cases of lenses with a negative (anticyclonic) initial angular velocity increases during the initial phase of their evolution reaching the largest values $h(t)$ and after that decreases to h_{crit}. The angular velocity of lens rotation $\omega(t)$ "exponentially" tends to $\omega(t) \to 0$. The lens semi-thickness $h(t)$, corresponding to the initial angular velocity $\omega_0 > 0$ (cyclonic rotation), quickly decreases during the first several days of the lens evolution, and after that the rate of $h(t)$ decreasing becomes significantly less and for the time period of about ~1000 days the lens semi-thickness $h(t)$ approaches to the critical value of about $h(t) \approx 1.1 \times h_{crit}$. The semi-thickness of the anti-cyclonic lens reaches the critical value of about $h(t) \approx 1.1 \times h_{crit}$ for the same temporal interval ~1000 days.

5. Conclusion

The lenses of the Mediterranean water (LMW), also known as Meddies, well distinguishable in the Atlantic Ocean water. The field observations devoted to study Meddies are presented in numerous publications and provide information on their origination, distribution, spatial scales and temporal dynamic activities. The salt-fingers and double-diffusion at the Meddies top and bottom borders may be considered as only mechanisms causing the Meddies disappearance as the thermal — saline mesoscale non-uniformities in the surrounding Atlantic Ocean waters. Taking into account the Medies' realistic scales it is shown that in temporal scales of about and less than a year the Meddies water mass may be considered as invariable. Then the Meddies conservation mass is valid in such temporal scales.

The Meddies (LMW) temporal variability analysis is carried out using the theoretical approach of intrusive lens in stratified fluid extended taking into account the Coriolis force. The Meddies (LMW) are considered with the center of gravity sitting at the level of equal density. The temporal variability occurs due to the resulting effect of the set of forces: the surplus pressure originated due to the density difference between the water inside the LMW and the ambient density field; the forces originated due to both the lens' rotation (centrifugal) and the Earth rotation (Coriolis); the forces caused by the internal wave radiation and the viscosity action. The temporal variability of LMW constitutes of two principal stages:

1) the initial, inviscid stage ("young lens"), when balance of forces is formed by the forces of inertia, the surplus pressure, the centrifugal force, the Carioles force and the force of wave resistance due to the internal wave radiation; the Coriolis force is a key factor supporting and keeping compact the anti-cyclonic LMW, the Meddies; it prevents the LMWs from breakup, limits their geometrical dimensions, affects the lens angular velocity variations. The cyclonic LMWs are destabilized by the Coriolis force, getting small thickness, and under certain conditions may disappear as a density anomaly already in the course of this stage;

2) the viscid stage ("old lens") is characterized by a slow decreasing of the LMW thickness up to its limit value, that is determined by the LMW initial thickness, the initial LMW stratification as well as ambient stratification; during the final period of the viscous stage the exchange of heat and salinity with ambient water-mass may, on a characteristic temporal scales about a year, significantly influence on the degenerations of the LMW as a density anomaly; at this stage the anti-cyclonic LMW, the Meddy, continues to have the anti-cyclonic rotation.

All the results discussed here relate to the conservation of the lens' bulk mass or the lens' of constant volume. The discussed numerical simulations allow presenting the dynamic features of the lens — Meddies as follows:

1. The existence of the lenses with cyclonic or anticyclonic rotations is supported theoretically. The lens with anticyclonic rotation has greater vertical size. An approximate interval of the initial angular velocities ω_0 of lens rotation is $-1.25f < \omega_0 < 0.75f$.

2. During the lens temporal evolution the lens semi-thickness tends to its critical value, which depends on the initial lens thickness and the lens mixing parameter σ. The angular velocity $\omega(t)$ of lens rotation tends to zero and the density gradient inside the lens to the ambient value. The "young lens" has greater the thickness, less the horizontal size and greater the angular velocity of rotation than "old" ones.

3. Lifetime of a lens, its dimensions and its angular velocity of rotation depend on the difference between the density stratification inside and outside the lens — greater stratification difference causes longer the lifetime of the lens and its angular velocity but the lens thickness becomes less.

4. The dynamic outcome of the initial values of angular velocity of lens rotation of the range $-f < \omega_0 < -0.5f$ is the growth of the lens' thickness $h(t)$ during the time interval of about 30–50 days. In the course of this time interval the thickness of the lens $h(t)$ may become greater than 1 km. The lens of such vertical size may be affected by the velocity shear of the ambient ocean currents, the topography of the bottom and the costal line as well the variability of the ambient density stratification.

5. The thickness of lens reaches its maximal value for the initial angular velocity $\omega_0 = -0.5f$.

6. A typical life time of lens is about 1–5 year. A dipole structure of lenses lives relatively long time, but the cyclonic lens may be hardly identified due to fast approaching to h_{crit}.

7. The complete degeneration of lens, as anomaly of the salinity and temperature by achievement h_{crit} and damping of the angular velocity, may occur mainly due to interactions the lens with the ambient mean currents. It may be considered as one of mechanisms creating the ocean vertical thermohaline fine structure.

8. At the "mature" lens stage ($t > 0.5$ year) the lens dynamics has a small sensitivity to the changes of the lens internal parameters. That increases reliability of the estimation of macro-scale heat and salinity exchanges due to lens transport of water with anomalous characteristics.

6. Acknowledgments

The authors are grateful to D.V. Chalikov, B.A. Kagan and V.A. Ryabchenko for valuable discussions on the subject of this study.

7. Financing

This research was performed in the framework of the state assignment (theme No. 0149–2019–0015).

Литература

1. *Yan Xiao-Hai*, *Young-Heon Jo*, *W. Timothy Liu*, *Ming-Xia He*. A New Study of the Mediterranean Outflow, Air–Sea Interactions, and Meddies Using Multisensor Data // Journal of Physical Oceanography. 2006. V. 36, N 4. P. 691–710.
2. *Bryden H.L.*, *Candela J.C.*, *Kinder T.H.* Exchange through the Strait of Gibraltar // Progress in Oceanography. 1994. V. 33. Pergamon. P. 201–248.
3. *Candela J.C.* Mediterranean Water and Global Circulation. Ocean Circulation and Climate: Observing and Modelling the Global Ocean / Eds. G. Siedler, J. Church, and J. Gould, Academic Press, 2001. P. 419–429.
4. *Jia Yanli*, *Andrew C. Coward*, *Beverly A. De Cuevas*, *David J. Webb*, *Sybren S. Drijfhout*. A Model Analysis of the Behavior of the Mediterranean Water in the North Atlantic // Journal of Physical Oceanography. 2007. V. 37, N 3. P. 764–786.

5. *Bower A.S.*, *Serra N.*, *Ambar I.* Structure of the Mediterranean Undercurrent and Mediterranean Water spreading around the southwestern Iberian Peninsula // Journal of Geophysical Research. 2002. 107 (C10). P. 3161.
6. *Richardson P.L.*, *Bower A.S.*, *Zenk W.* A census of meddies tracked by floats // Progress in Oceanography. 2000. V. 45. P. 209–250.
7. *Филюшкин Б.Н.*, *Плахин Е.А.* Экспериментальные исследования начальной стадии формирования линзы средиземноморской воды // Океанология. 1995. Т. 35, № 6. С. 875–882.
8. *Serra N.*, *Ambar I.*, *Kaase R.H.* Observations and numerical modeling of the Mediterranean outflow splitting and eddy generation // Deep Sea Res. 2005. II. 52. P. 383–408.
9. *McDowell S.E.*, *Rossby H.T.* Mediterranean Water: An Intense Mesoscale Eddy off the Bahamas // Science. 1978. V. 202. 4372. P. 1085–1087.
10. *Dugan J.P.*, *Mied R.P.*, *Mignerey P.C.*, *Schuetz A.P.* Compact, Intrathermocline Eddies in the Sargasso Sea // Journal of Geophysical Research. 1982. N 1C. P. 385–393.
11. *Armi L.*, *Zenk W.* Large Lenses of Highly Saline Mediterranean Water // Journal of Physical Oceanography. 1984. V. 14, № 10. P. 1560–1576.
12. *Richardson P.L.*, *Walsh D.*, *Armi L.*, *Schröder M.*, *Price J.F.* Tracking three Meddies with SOFAR floats // Journal of Physical Oceanography. 1989. V. 19. P. 371–383.
13. *Richardson P.L.*, *McCartney M.S.*, *Maillard C.* A search for Meddies in historical data // Dynamics of Atmospheres and Oceans. 1991. V. 15. P. 241–265.
14. *Käse R.H.*, *Zenk W.* Structure of the Mediterranean Water and Meddy characteristics in the northeastern Atlantic / W. Krauss, Warmwatersphere of the North Atlantic Ocean Berlin, Gebrüder Borntraeger, 1996. P. 365–395.
15. *Richardson P.L.*, *Tychensky A.* Meddy trajectories in the Canary Basin measured during the Semaphore Experiment, 1993–1995 // Journal of Geophysical Research. 1998. V. 103. P. 25029–25045.
16. *Paillet Jerome*, *B. Le Cann*, *Xavier Carton, Yves Morel*, *Alain Serpette*. Dynamics and Evolution of a Northern Meddy // Journal of Physical Oceanography. 2002. V. 32, N 1. P. 55–79.
17. *Bower A.S.*, *Armi L.*, *Ambar I.* Lagrangian Observations of Meddy Formation During a Mediterranean Undercurrent Seeding Experiment // Journal of Physical Oceanography. 1997. V. 27. P. 2545–2575.
18. *Федоров К.Н.* Введение. Внутритермоклинные вихри — специфический тип океанских вихрей с ядром // Внутритермоклинные вихри в океане / Под ред. К.Н. Федорова. М.: Институт Океанологии АН СССР, 1986. С. 5–7.
19. *Voropayev S.I.*, *Afanasyev Y.D.* Vortex Structures in a Stratified Fluid: Order from Chaos. Chapman and Hall, 1994. 230 p.
20. *Afanasyev Y.D.* Formation of vortex dipoles // Physics of Fluids. 2006. V. 18, 037103. P. 1–9.
21. *Benilov A.*, *Safray A.*, *Filyushkin B.*, *Kojelupova N.* On Meddy Nonlinear Dynamics // 37th Annual Mid-Atlantic Bight Physical Oceanography and Meteorology / Stevens Institute of Technology. Hoboken, NJ. 2010. P. 20–21.
22. *Зацепин А.Г.* О коллапсе стратифицированных областей // ДАН. 1982. Т. 265, № 2. С. 460–463.
23. *Afanasyev Y.D.*, *Filippov I.A.* Generation of intermediate water vortices in a rotating stratified fluid: Laboratory model // Journal of Geophysical Research. 1996. V. 101, N C8. P. 18,167–18,174.
24. *Hedstrom K.*, *Armi L.* An Experimental Study of Homogeneous Lenses in a stratified rotating fluid // J. Fl. Mech. 1988. V. 191. P. 535–556.
25. *Chushman-Roisin B.* Linear Stability of Large, Elliptical Warm-Core Rings // Journal of Physical Oceanography. 1986. V. 16. P. 1158–1164.
26. *Bashmachnikov I.*, *Machin F.*, *Mendonca A.*, *Martins A.* In situ and remote sensing signature of meddies east of the mid-Atlantic ridge // Journal of Geophysical Research. 2009. V. 114. P. C05018. doi: 10.1029 /2008JC005032
27. *Armi L.*, *Hebert D.*, *Oakey N.*, *Price J.*, *Richardson P.*, *Rossby H.*, *Ruddick B.* Two years in the life of a Mediterranean salt lens // Journal of Physical Oceanography. 1989. V. 19. N 3. P. 354–370.
28. *Schultz Tokos K.*, *Rossby H.T.* Kinematics and dynamics of a Mediterranean salt lens // Journal of Physical Oceanography. 1991. V. 21. P. 879–892.
29. *Pingree R.D.*, *LeCann B.* A shallow Meddy (a Smeddy) from the secondary Mediterranean salinity maximum // Journal of Geophysical Research. 1993. V. 98. P. 20169–20185.
30. *Pingree R.D.*, *LeCann B.* Structure of a Meddy (Bobby 92) southeast of the Azores // Deep-Sea Research I. 1993. V. 40. P. 2077–2103.
31 *Prater M.D.*, *Sanford T.B.* A Meddy off Cape St. Vincent. Part I: description // Journal of Physical Oceanography. 1994. V. 24. P. 1572–1586.
32. *Tychensky A.*, *Carton X.* Hydrological and dynamical characterization of Meddies in the Azores region: a paradigm for baroclinic vortex dynamics // Journal of Geophysical Research. 1998. V. 103. P. 25061–25079.
33. *Stammer D.*, *Hinrichsen H.-H.*, *Käse R.H.* Can Meddies be detected by satellite altimetry? // Journal of Geophysical Research. 1991. V. 96. P. 7005–7014.

34. *Ruddick B.* Intrusive mixing in a Mediterranean salt lens — intrusion slopes and dynamical mechanisms // Journal of Physical Oceanography. 1992. V. 22. P. 1274–1285.
35. *Nandi P.*, *Holbrook S.*, *Pearse S.*, *Paramo P.*, *Schmitt R.* Seismic reflection imaging of water mass boundaries in the Norwegian Sea // Geophys. Res. Lett. 2004. V. 31, L23311. doi: 10.1029/2004GL021325
36. *Nakamura Y.*, *Noguchi T.*, *Tsuji T.*, *Itoh S.*, *Niino H.*, *Matsuoka T.* Simultaneous seismic reflection and physical oceanographic observations of oceanic fine structure in the Kuroshio extension front // Geophys. Res. Lett. 2006. V. 33, L23605. doi: 10.1029/2006GL027437
37. *Biescas B.*, *Sallarès V.*, *Pelegrì J.L.*, *Machín F.*, *Carbonell R.*, *Buffett G.*, *Dañobeitia J.J.*, *Calahorrano A.* Imaging meddy fine structure using multichannel seismic data // Geophys. Res. Lett. 2008. V. 35, L11609. doi: 10.1029/2008GL033971
38. *Ruddick B.*, *Song H.*, *Dong C.*, *Pinheiro L.* Water column seismic images as maps of temperature gradient // Oceanography. 2009. V. 22. P. 192–205.
39. *Buffett G.G.*, *Biescas B.*, *Pelegri J.L.*, *Machin F.*, *Sallares V.*, *Carbonell R.*, *Klaeschen D.*, *Hobbs R.W.* Seismic reflection along the path of the Mediterranean Undercurrent // Cont. Shelf Res. 2009. V. 29. P. 1848–1860.
40. *Buffett G.G.*, *Hurich C.A.*, *Vsemirnova E.A.*, *Hobbs R.W.*, *Sallares V.*, *Carbonell R.*, *Klaeschen D.*, *Biescas B.* Stochastic Heterogeneity Mapping Around a Mediterranean Salt Lens // Ocean Sci. 2010. V. 6. P. 423–429.
41. *Филюшкин Б.Н.* Исследование внутритермоклинных линз средиземноморского происхождения (16 рейс нис «Витязь». 3 июня — 16 сентября 1988 г.) // Океанология. 1989. Т. 29, № 4. С. 296–298.
42. *Максименко Н.А.* Сравнительный анализ течений и полей плотности морской воды в средиземноморских линзах по данным «Мезополигона» // Гидрофизические исследования по программе «Мезополигон». М.: Наука, 1988. С. 69–76.
43. *Филюшкин Б.Н.*, *Демидов Д.Л.*, *Сарафанов А.А.*, *Кожелупова Н.Г.* Особенности формирования и распространения средиземноморской водной массы на промежуточных глубинах Атлантического океана // Водные массы океанов и морей. М.: Макс пресс, 2007. С. 92–129.
44. *Иванов Ю.А.*, *Корт В.Г.*, *Шаповалов С.М.*, *Щербинин А.Д.* Мезомасштабные интрузионные линзы // Гидрофизические исследования по программе «Мезополигон». М.: Наука, 1988. С. 41–46.
45. *Kostianoy A.G.*, *Belkin G.M.* A survey of observations on intrathermocline eddies in the world ocean. // Mesoscale/synoptic coherent structure in geophysical turbulence. Proc. of the 20-th Int. Liege Colloq. on ocean hydrodynamic. / Ed. J.C.J. Nihoul, B.M. Jamaat. Elsevier. 1989. P. 821–841.
46. *Richardson P.L.*, *Bower A.S.*, *Zenk W.* Summary of Meddies Tracked by Floats // International WOCE Newsletter. 1999. N 34. P. 18–20.
47. *Алейник Д.А.*, *Плахин Е.А.*, *Филюшкин Б.Н.* К механизму формирования внутритермоклинных линз в районе каньонов континентального склона Кадисского залива // Океанология. 1998. Т. 38. № 5. С. 645–653.
48. *Дыхно Л.А.*, *Морозов Е.Г.*, *Никитин С.В. и др.* О разрушении линзы средиземноморской воды при взаимодействии с рельефом дна // Океанология. 1991. Т. 31, № 1. С. 55–61.
49. *Шапиро Г.И.*, *Мещанов С.Л.*, *Емельянов М.В.* Линза средиземноморских вод после столкновения с подводными горами // Океанология. 1992. Т. 32, № 3. С. 420–427.
50. *Алейник Д.Л.* Структура и динамика средиземноморской линзы и Азорской фронтальной зоны осенью 1993 г. // Океанология 1998. Т. 38, № 3. С. 349–360.
51. *Филюшкин Б.Н.*, *Алейник Д.Л.*, *Грузинов В.И.*, *Кожелупова Н.Г.* Динамическое разрушение средиземноморских линз в Атлантическом океане // ДАН. 2002. Т. 387, № 4. С. 545–548.
52. *Шапиро Г.И.* Динамика изолированного внутритермоклинного вихря // Океанология. 1986. Т. 26, № 1. С. 21–27.
53. *Ruddick B.R.* Anticyclonic lenses in large scale strain and shear // Journal of Physical Oceanography. 1987. V. 17. P. 741–749.
54. *Бенилов А.Ю.*, *Гаврилин В.Л.* Островки турбулентности в океанском пикноклине // Океанология. 1988. Т. 28, № 6. С. 700–705.
55. *Бенилов А.Ю.* О разрушении перемешанных областей в океанском пикноклине // Океанология. 1989. Т. 29, № 1. С. 33–39.
56. *Benilov A.Y.* Some Problems of Nonequilibrium Turbulence in the Nonsteady Turbulent Boundary Layers of the Ocean and Atmosphere // The Office of Naval Research, State-of-the-Art Workshop on Nonequilibrium Turbulence, March 10–12, 1993. Arizona State University, Tempe, Arizona. 1993. 85287–6106. P. 92–93.
57. *Лавровский Э.К.*, *Семенова И.П.*, *Слезкин Л.Н.*, *Фомин В.В.* Средиземноморские линзы — жидкие гироскопы в океане // ДАН. 2000. Т. 375, № 1. С. 42–45.
58. *Sokolovskiy M.A.*, *Filyushkin B.N.*, *Xavier J. Carton*. Dynamics of intrathermocline vortices in a gyre flow over a seamount chain // Ocean Dynamics. Springer, 2013. P. 3–22. doi: 10.1007/s10236–013–0628-y
59. *Островский А.Г.*, *Питербарг Л.И.* Авторегрессионная модель поля аномалий температуры на поверхности моря // Океанология. 1985. Т. 25, № 3. С. 333–334.

60. *Maas L.R.M.*, *Zahariev K.* An exact, stratified model of a meddy // Dyn. Atm. and Oceans. 1996. V. 24. Iss. 1–4. P. 215–225.
61. *Monin A.S.*, *Ozmidov R.V.* Turbulence in the Ocean // D. Reidel Publishing Company. 1985, 250 p.
62. *Barenblatt G.I.* Scaling, Self-similarity, and Intermediate Asymptotics // Cambridge University Press, 1996, 386 p.

References

1. *Yan Xiao-Hai*, *Young-Heon Jo*, *W. Timothy Liu*, *Ming-Xia He*. A New Study of the Mediterranean Outflow, Air–Sea Interactions, and Meddies Using Multisensor Data. *Journal of Physical Oceanography*. 2006, 36, 4, 691–710.
2. *Bryden H.L.*, *Candela J.C.*, *Kinder T.H.* Exchange through the Strait of Gibraltar. *Progress in Oceanography*. 1994, 33, Pergamon, 201–248.
3. *Candela J.C.* Mediterranean Water and Global Circulation. Ocean Circulation and Climate: Observing and Modelling the Global Ocean. / Eds. G. Siedler, J. Church, and J. Gould, *Academic Press*, 2001, 419–429.
4. *Jia Yanli*, *Andrew C. Coward*, *Beverly A. De Cuevas*, *David J. Webb*, *Sybren S. Drijfhout*. A Model Analysis of the Behavior of the Mediterranean Water in the North Atlantic. *Journal of Physical Oceanography*. 2007, 37, 3, 764–786.
5. *Bower A.S.*, *Serra N.*, *Ambar I.* Structure of the Mediterranean Undercurrent and Mediterranean Water spreading around the southwestern Iberian Peninsula. *Journal of Geophysical Research*. 2002, 107(C10), 3161.
6. *Richardson P.L.*, *Bower A.S.*, *Zenk W.* A census of meddies tracked by floats. *Prog. Oceanogr.* 2000, 45, 209–250.
7. *Filyushkin B.N.*, *Plakhin E.A.* Experimental study of the first stage of Mediterranean water lens formation. *Oceanology*. 1996, 35, 6, 797–804.
8. *Serra N.*, *Ambar I.*, *Kaase R.H.* Observations and numerical modeling of the Mediterranean outflow splitting and eddy generation. *Deep Sea Res.* 2005, II, 52, 383–408.
9. *McDowell S.E.*, *Rossby H.T.* Mediterranean Water: An Intense Mesoscale Eddy off the Bahamas. *Science*. 1978, 202, 4372, 1085–1087.
10. *Dugan J.P.*, *Mied R.P.*, *Mignerey P.C.*, *Schuetz A.P.* Compact, Intrathermocline Eddies in the Sargasso Sea. *Journal of Geophysical Research*. 1982, N 1C, 385–393.
11. *Armi L.*, *Zenk W.* Large Lenses of Highly Saline Mediterranean Water. *Journal of Physical Oceanography*. 1984, 14, 10, 1560–1576.
12. *Richardson P.L.*, *Walsh D.*, *Armi L.*, *Schröder M.*, *Price J.F.* Tracking three Meddies with SOFAR floats. *Journal of Physical Oceanography*. 1989, 19, 371–383.
13. *Richardson P.L.*, *McCartney M.S.*, *Maillard C.* A search for Meddies in historical data. *Dynamics of Atmospheres and Oceans*. 1991, 15, 241–265.
14. *Käse R.H.*, *Zenk W.* Structure of the Mediterranean Water and Meddy characteristics in the northeastern Atlantic / W. Krauss, *Warmwatersphere of the North Atlantic Ocean Berlin*, 1996, *Gebrüder Borntraeger*, 365–395.
15. *Richardson P.L.*, *Tychensky A.* Meddy trajectories in the Canary Basin measured during the Semaphore Experiment, 1993–1995. *Journal of Geophysical Research*. 1998, 103, 25029–25045.
16. *Paillet Jerome*, *B. Le Cann*, *Xavier Carton*, *Yves Morel and Alain Serpette*. Dynamics and Evolution of a Northern Meddy. *Journal of Physical Oceanography*. 2002, 32, 1, 55–79.
17. *Bower A.S.*, *Armi L.*, *Ambar I.* Lagrangian Observations of Meddy Formation During a Mediterranean Undercurrent Seeding Experiment. *Journal of Physical Oceanography*. 1997, 27, 2545–2575.
18. *Fedorov K.N.* (Editor). Intrathermocline eddies in the ocean. *Moscow*, *IO RAS*, 1986, 5–7.
19. *Voropayev S.I.*, *Afanasyev Y.D.* Vortex Structures in a Stratified Fluid: Order from Chaos. *Chapman and Hall*, 1994. 230 p.
20. *Afanasyev Y.D.* Formation of vortex dipoles. *Physics of Fluids*. 2006, 18, 037103, 1–9.
21. *Benilov A.*, *Safray A.*, *Filyushkin B.*, *Kojelupova N.* On Meddy Nonlinear Dynamics. *37th Annual Mid-Atlantic Bight Physical Oceanography and Meteorology*. *Stevens Institute of Technology*. *Hoboken*, *NJ*. 2010, 20–21.
22. *Zatsepin A.G.* About a collapse of stratified spots. *Doklady AN USSR*. 1982, 265, 2, 460–463 (in Russian).
23. *Afanasyev Y.D.*, *Filippov I.A.* Generation of intermediate water vortices in a rotating stratified fluid: Laboratory model. *Journal of Geophysical Research*. 1996, 101, C8, 18,167–18,174.
24. *Hedstrom K.*, *Armi L.* An Experimental Study of Homogeneous Lenses in a stratified rotating fluid. *J. Fl. Mech*. 1988, 191, 535–556.
25. *Chushman-Roisin B.* Linear Stability of Large, Elliptical Warm-Core Rings. *Journal of Physical Oceanography*.1986, 16, 1158–1164.
26. *Bashmachnikov I.*, *Machin F.*, *Mendonca A.*, *Martins A.* In situ and remote sensing signature of meddies east of the mid-Atlantic ridge. *Journal of Geophysical Research*. 2009, 114, C05018. doi: 10.1029/2008JC005032
27. *Armi L.*, *Hebert D.*, *Oakey N.*, *Price J.*, *Richardson P.*, *Rossby H.*, *Ruddick B.* Two years in the life of a Mediterranean salt lens. *Journal of Physical Oceanography*. 1989, 19, 3, 354–370.

28. *Schultz Tokos K.*, *Rossby H.T.* Kinematics and dynamics of a Mediterranean salt lens. *Journal of Physical Oceanography*. 1991, 21, 879–892.
29. *Pingree R.D.*, *LeCann B.* A shallow Meddy (a Smeddy) from the secondary Mediterranean salinity maximum. *Journal of Geophysical Research*. 1993, 98, 20169–20185.
30. *Pingree R.D.*, *LeCann B.* Structure of a Meddy (Bobby 92) southeast of the Azores. *Deep-Sea Research I*. 1993, 40, 2077–2103.
31. *Prater M.D.*, *Sanford T.B.* A Meddy off Cape St. Vincent. Part I: description. *Journal of Physical Oceanography*. 1994, 24, 1572–1586.
32. *Tychensky A.*, *Carton X.* Hydrological and dynamical characterization of Meddies in the Azores region: a paradigm for baroclinic vortex dynamics. *Journal of Geophysical Research*. 1998, 103, 25061–25079.
33. *Stammer D.*, *Hinrichsen H.-H.*, *Käse R.H.* Can Meddies be detected by satellite altimetry? *Journal of Geophysical Research*. 1991, 96, 7005–7014.
34. *Ruddick B.* Intrusive mixing in a Mediterranean salt lens — intrusion slopes and dynamical mechanisms. *Journal of Physical Oceanography*. 1992, 22, 1274–1285.
35. *Nandi P.*, *Holbrook S.*, *Pearse S.*, *Paramo P.*, *Schmitt R.* Seismic reflection imaging of water mass boundaries in the Norwegian Sea. *Geophys. Res. Lett.* 2004, 31, L23311. doi: 10.1029/2004GL021325
36. *Nakamura Y.*, *Noguchi T.*, *Tsuji T.*, *Itoh S.*, *Niino H.*, *Matsuoka T.* Simultaneous seismic reflection and physical oceanographic observations of oceanic fine structure in the Kuroshio extension front. *Geophys. Res. Lett*. 2006, 33, L23605, doi: 10.1029/2006GL027437
37. *Biescas B.*, *Sallarès V.*, *Pelegrì J.L.*, *Machín F.*, *Carbonell R.*, *Buffett G.*, *Dañobeitia J.J.*, *Calahorrano A.* Imaging meddy fine structure using multichannel seismic data. *Geophys. Res. Lett.* 2008, 35, L11609. doi: 10.1029/2008GL033971
38. *Ruddick B.*, *Song H.*, *Dong C.*, *Pinheiro L.* Water column seismic images as maps of temperature gradient. *Oceanography*. 2009, 22, 192–205.
39. *Buffett G.G.*, *Biescas B.*, *Pelegri J.L.*, *Machin F.*, *Sallares V.*, *Carbonell R.*, *Klaeschen D.*, *Hobbs R.W.* Seismic reflection along the path of the Mediterranean Undercurrent. *Cont. Shelf Res.* 2009, 29, 1848–1860.
40. *Buffett G.G.*, *Hurich C.A.*, *Vsemirnova E.A.*, *Hobbs R.W.*, *Sallares V.*, *Carbonell R.*, *Klaeschen D.*, *Biescas B.* Stochastic Heterogeneity Mapping Around A Mediterranean Salt Lens. *Ocean Sci*. 2010, 6, 423–429.
41. *Filyushkin B.N.* Investigation of intrathermocline lenses of Mediterranean origin (Cruise 16 of R/V "Vityaz", June 3 — September 16, 1988). *Oceanology*. 1989, 29, 4, 535–536.
42. *Maksimenko N.A.* A comparative analysis of currents and seawater density fields into Mediterranean lenses by the data of "Mezopoligon". *Proceedings* "*Hydrophysical studies at "Mesopoligon" program". Moscow*, *Nauka*, 1988, 69–76 (in Russian).
43. *Filyushkin B.N.*, *Demidov A.N.*, *Sarafanov A.A.*, *Kozhelupova N.G.* The peculiarity of the formation and spreading Mediterranean water mass at intermediate depths of the Atlantic Ocean. *Waters masses of the oceans and sea. MAX Press*, *Moscow*, 2007, 92–129 (in Russian).
44. *Ivanov Yu.A.*, *Kort V.G.*, *Shapovalov S.M.*, *Scherbinin A.D.* Mezo-scale Intrusion lenses. *Proceedings* "*Hydrophysical studies at "Mesopoligon" program". Moscow*, *Nauka*, 1988, 41–46 (in Russian).
45. *Kostianoy A.G.*, *Belkin G.M.* A survey of observations on intrathermocline eddies in the world ocean. *Mesoscale/synoptic coherent structure in geophysical turbulence. Proc. of the 20-th Int. Liege Colloq. on ocean hydrodynamic* / Ed. J.C.J. Nihoul, B.M. Jamaat. *Elsevier*. 1989, 821–841.
46. *Richardson P.L.*, *Bower A.S.*, *Zenk W.* Summary of Meddies Tracked by Floats. *International WOCE Newsletter*. 1999, 34, 18–20.
47. *Aleinik D.L.*, *Plakhin E.A.*, *Filyushkin B.N.* On the mechanism of formation of intra thermocline lenses in the canyon area of the gulf Cadiz continental slope. *Oceanology*. 1998, 38, 5, 645–653 (in Russian).
48. *Dykhno L.A. et al.* Breakup of lenses of Mediterranean water on interaction with bottom relief. *Oceanology*. 1991, 31, 1, 38–41.
49. *Shapiro G.I.*, *Meshchanov S.L.*, *Yemel'yanov M.V.* Mediterranean water lens after a collision with seamounts. *Oceanology*. 1992, 32, 3, 279–283.
50. *Aleinik D.L.* The structure an evolution of a meddy and Azores frontal zone in autumn 1993. *Ac. Sci. USSR. Oceanology*. 1998, 38, 3, 312–322.
51. *Filyushkin B.N.*, *Aleinik D.L.*, *Gruzinov B.M.*, *Kozhelupova N.G.* Dynamic degradation of the Mediterranean lenses in the Atlantic Ocean. *Doklady Earth Sciences*. 2002, 387a, 9, 1079–1082.
52. *Shapiro G.I.* Dynamics of an isolated intrathermocline eddy. *Oceanology*. 1986, 26, 1, 12–15.
53. *Ruddick B.R.* Anticyclonic lenses in large scale strain and shear. *Journal of Physical Oceanography*. 1987, 17, 741–749.
54. *Benilov A. Yu.*, *Gavrilin B.L.* Island Turbulence of the Ocean Pycnocline. *Ac. Sci. USSR. Oceanology*. 1988, 28, 6, 700–705 (in Russian).
55. *Benilov A. Yu*. On the Mixed Regions Collapse in the Ocean Pycnocline. *Ac. Sci. USSR. Oceanology*. 1989, 29, 1, 33–39 (in Russian).

56. *Benilov A.Y.* Some Problems of Nonequilibrium Turbulence in the Nonsteady Turbulent Boundary Layers of the Ocean and Atmosphere. *The Office of Naval Research*, *State-of-the-Art Workshop on Nonequilibrium Turbulence*, *March 10–12, 1993. / Arizona State University*, *Tempe*, *Arizona*. 1993, 85287–6106, 92–93.
57. *Lavrovsky E.K.*, *Semenova I.P.*, *Slyezkin L.N.*, *Fominih V.V.* Mediterranean lenses — liquid gyroscopes in the Oceans. *Doklady RAS*. 2000, 375, 1, 42–45 (in Russian).
58. *Sokolovskiy M.A.*, *Filyushkin B.N.*, *Xavier J. Carton*. Dynamics of intrathermocline vortices in a gyre flow over a seamount chain. *Ocean Dynamics*, *Springer*, 2013, 3–22. doi: 10.1007/s10236–013–0628-y
59. *Ostrovsky A.G.*, *Piterbarg L.I.* Autoregressian model of sea surface temperature anomaly field in the North Atlantic. *Oceanology*. 1985, 25, 3, 333–334 (in Russian).
60. *Maas L.R.M.*, *Zahariev K.* An exact, stratified model of a meddy. *Dyn. Atm. and Oceans*. 1996, 24, 1–4, 215–225.
61. *Monin A.S.*, *Ozmidov R.V.* Turbulence in the Ocean. *D. Reidel Publishing Company*. 1985, 250 p.
62. *Barenblatt G.I.* Scaling, Self-similarity, and Intermediate Asymptotics. *Cambridge University Press*. 1996, 386 p.